Interest of the regular 2-state model for the description of unary liquids: Presentation of the formalism

P. Benigni

Interest of the regular 2-state model for the description of unary liquids: presentation of the formalism

P. Benigni, Aix Marseille Univ., Université de Toulon, CNRS, IM2NP, Marseille, France

Institut Matériaux Microélectronique Nanosciences de Provence, UMR 7334 CNRS – Aix-Marseille Université, FST St Jérôme, Service 251, avenue Normandie-Niémen, 13397 Marseille – Cedex 20 (France)

Email address: p.benigni@univ-amu.fr

Abstract

The ideal 2-state model is exclusively used for describing the liquid phase in 3rd generation CALPHAD work. However, not all types of liquids can be described using an ideal 2-state model and for liquids qualified as fragile, a regular 2-state model appears to be a more promising modelling solution. The formalism and phase diagram of the regular model are presented with particular emphasis on the pressure variable. The main characteristics of the regular 2-state model are illustrated through a parametric study and the two test cases of tellurium and water taken from literature studies. The present article suggests that, compared to its ideal counterpart, the regular 2-state model may represent a valuable complementary modeling tool that considerably broadens the spectrum of phenomena that can be described. This model should only be used if it significantly improves the description compared to the ideal model, and its applicability in a multicomponent system should also be verified.

Graphical abstract

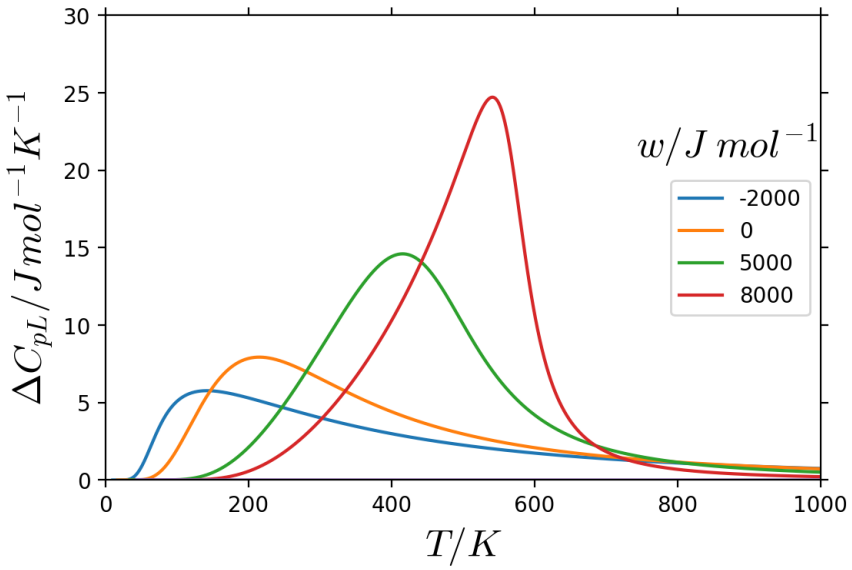

Keywords

Thermodynamics; 2-state model; regular solution; liquid; glass.

Introduction

The ideal 2-state model, extensively described in [1] [2] and [3] is now of common use to describe the liquid phase in the development of CALPHAD 3rd generation databases. Up to now, this ideal model has been applied to an increasing number of elements, e.g. Al [4] [5], Au [6], B [7], C [5] [8], Co [9], Fe [7] [10] [11], In [12], Mn [13], Nb [14], Pb [15], Sn [16] [17], W [18], Zn [4], some binaries e.g. Al-C [5], Al-Zn [4], B-Fe [7], Pb-Sn [19], C-W [20] and at least one ternary, B-Fe-Nb [14]. The above, yet not exhaustive, list shows that most of ongoing developments are focused on metallic elements and metal based systems. Some attempts have recently been made to extend the model to unary oxides such as B_2O_3 [21], CaO [22], SiO_2 [23] and GeO_2 [24].

To judge the applicability of a thermodynamic model, glass forming liquids offer more discriminating tests than easily crystallizing liquids, as heat capacity of the former can be measured not only above the melting point, but also over a wide interval in the supercooling range. In addition, data on the heat capacity of glass is also available down to low temperatures.

The fragility index allows glass forming liquids to be classified between the so-called "strong" and "fragile" extremes. For a definition of the fragility, the reader is referred to the work of Angell [25] [26] and the fragility index values for an extensive list of liquids can be found in [27]. In this classification, the least fragile liquids are called strong. The viscosity of a strong liquid has an Arrhenian dependence on temperature, which means that the activation energy of the viscous flow remains constant from high temperatures down to the glass transition temperature T_g. In contrast, when cooling fragile liquids from high temperatures, the increase in viscosity is initially small and then starts to increase very steeply in the vicinity of T_g, reflecting a strong increase in the activation energy of viscous flow in the glass transition range. This deviation from the Arrhenian behavior is sometimes called "super-Arrhenian". It is also known that this kinetic fragility is closely related to configurational entropy, and thus to thermodynamics. Since the seminal paper of Adam & Gibbs [28], this connection has been extensively investigated by numerous authors such as Martinez & Angell [29], Speedy [30], Johari [31] and Sastry [32]. One difficulty in the clarification of the correlation between the kinetic and thermodynamic aspects of the glass transition lies in the fact that the configurational entropy cannot be measured directly, but only estimated indirectly and imperfectly [33] by calculating the excess entropy of the liquid over the crystal entropy or alternatively the glass entropy, or calculated with a thermodynamic model.

With these considerations in mind, it should be noted that all the elements mentioned at the beginning of the introduction do not form glasses easily and that, in addition, a large fraction of them are high melting point elements on which it remains very difficult to measure the heat capacity over a wide temperature range. On the other hand, B_2O_3, GeO_2 and SiO_2 do form glasses but they all belong to the category of strong-liquids [34] and therefore do not represent by themselves all the phenomenology that can be found in liquids.

The purpose of this paper is to identify which type of 2-state model might be most appropriate for a given type of liquid. Indeed, not all types of liquids can be described using an ideal 2-state model and for liquids qualified as fragile, a regular 2-state model appears to be a more promising modelling solution. In the CALPHAD literature, the interest in using a non-ideal, sub-regular, two-state model had already been perceived by Golczewski et al. [35]. The present work represents an attempt to convince the reader of the interest of using a regular 2-state model in specific cases. The structure of the article will be as follows.

The first section will be devoted to the analysis of the ideal 2-state model. Even if excellent comprehensive presentations and analyses of this model are already available [1] [2] [3], it seems relevant to us to propose here a new analysis, complementary to the one carried out in our previous study [21] and to those in the literature. We insist in this analysis, on the role of each of the parameters which intervene in the difference of Gibbs free energy between the 2-states on the behavior of the model.

The second section will be focused on the parametrization of the ideal model. We propose here a kind of "meta-analysis" based on a comparison of optimized parameter sets extracted from different studies published in the literature. For new users of the model, these first two sections of the article may have the additional interest of clarifying certain modeling choices and helping to identify some recommendations or good practices when optimizing the parameters.

On the basis of a concise review of glass research literature, in the third section we list the main limitations of the ideal 2-state model and identify the regular 2-state model as a more appropriate modeling choice in certain situations.

The basic equations and the temperature composition phase diagram of the regular 2-state model will be presented in the fourth section and the most useful thermodynamic functions under atmospheric pressure are calculated in the fifth section.

The description of the behavior of liquids under high pressure is one of the main reasons for using the regular two-state model. The introduction of the pressure variable into the model is therefore the subject of the sixth section in which the pressure-temperature phase diagram is also presented.

Two examples, tellurium and water, are selected from the literature are presented in the seventh section to illustrate in a more concrete way the interest of the model.

A general discussion is presented in the eighth section before a final concise conclusion.

1 Analysis of the ideal 2-state model

The basic ideas behind the model are i) that the liquid is composed of two types of entities or structural units, A and B, and ii) that they form an ideal solution.

First, for the sake of completeness, we recall the equations of the model derived many times (e.g. [1], [21]).

The Gibbs energy of the ideal A-B liquid solution reads:

$$G_L = \xi_A G_A^\circ + \xi_B G_B^\circ + RT(\xi_A ln\xi_A + \xi_B ln\xi_B) \quad (1)$$

The mole fraction of B units, denoted $\xi_B (= \xi)$, is selected to play the role of an internal non-conservative thermodynamic variable that defines the state of the liquid under given external temperature and pressure conditions. The notation ξ is adopted to emphasise the difference in nature between this variable and the usual mole fraction $x_B\ (= x)$ in a classical binary solution, which is an external and conservative thermodynamic variable, whose value is controlled by the experimenter.

By keeping a single $\xi_B = 1 - \xi_A = \xi$ internal compositional variable, the Gibbs energy is rewritten:

$$G_L = (1-\xi)G_A^\circ + \xi G_B^\circ + RT((1-\xi)\ln(1-\xi) + \xi\ln\xi) \quad (2)$$

We introduce the Gibbs energy difference ΔG_d between the two states and express it as the sum of its enthalpic and entropic contributions:

$$\Delta G_d = G_B^\circ - G_A^\circ = \Delta H_d - T\Delta S_d \quad (3)$$

The configurational Gibbs energy of the liquid now reads:

$$\Delta G_L = G_L - G_A^\circ = \xi\Delta G_d + RT((1-\xi)\ln(1-\xi) + \xi\ln\xi) \quad (4)$$

The internal equilibrium condition:

$$\left(\frac{\partial \Delta G_L}{\partial \xi}\right)_{\xi=\xi_e} = 0 \quad (5)$$

Yields the following equation:

$$\Delta G_d = -RTln\frac{\xi_e}{(1-\xi_e)} \tag{6}$$

In which the "e" subscript of ξ_e means that the mole fraction of B is taken at equilibrium value.

This equation represents a law of mass action for the pseudo-chemical reaction:

$$A \rightleftharpoons B \tag{7}$$

Equation (6) can be inverted to give the following explicit expression of ξ_e:

$$\xi_e = \frac{exp\left(-\frac{\Delta G_d}{RT}\right)}{1 + exp\left(-\frac{\Delta G_d}{RT}\right)} \tag{8}$$

An alternative form of equation (8) that is more meaningful for analyzing the asymptotic behavior of ξ_e reads:

$$\xi_e = \frac{1}{1 + exp\left(\frac{\Delta G_d}{RT}\right)} \tag{9}$$

The curve $\xi_e(T)$ given by equations (8) or (9) is called the "excitation profile" by Angell [36] and has a sigmoid shape which goes from 0 at 0 K to an asymptotic value in the high temperature limit which depends on the analytical expression of ΔG_d as will be shown in the following.

All thermodynamic functions can then be calculated, starting with the entropy:

$$\Delta S_L = S_L - S_A^\circ = -\left(\frac{\partial \Delta G}{\partial T}\right)_p = \xi \Delta S_d - R((1-\xi)\ln(1-\xi) + \xi \ln \xi) \tag{10}$$

Then the configurational enthalpy:

$$\Delta H_L = H_L - H_A^\circ = \Delta G_L + T\Delta S_L = \xi \Delta H_d \tag{11}$$

And the configurational heat capacity (see e.g. eq. (8) of [3]):

$$\Delta C_{pL} = \left(\frac{\partial \Delta H_d}{\partial T}\right)_p \xi_e + \Delta H_d \left(\frac{\partial \xi_e}{\partial T}\right)_p \tag{12}$$

Differentiating eq. (9) with respect to temperature gives:

$$\left(\frac{\partial \xi_e}{\partial T}\right)_p = \frac{\Delta H_d}{RT^2}\xi_e(1-\xi_e) \tag{13}$$

Which allows to calculate the second term on the right side of eq. (12).

Differentiating eq. (13) with respect to temperature and applying the condition:

$$\left(\frac{\partial^2 \xi_e}{\partial T^2}\right)_p = 0 \tag{14}$$

Yields a relation between the value of the fraction of excited units at the inflexion point ($\xi_{e,inf}$) of the excitation profile and the corresponding temperature (T_{inf}) which remains to be evaluated:

$$\xi_{e,inf} = \frac{1}{2} - \frac{RT_{inf}}{\Delta H_d} + \frac{1}{2}\left(\frac{RT_{inf}}{\Delta H_d}\right)^2 \frac{1}{R}\left(\frac{\partial \Delta H_d}{\partial T}\right)_p \tag{15}$$

To determine the temperature and value of the heat capacity maximum, it is necessary to calculate the partial derivative of the heat capacity:

$$\left(\frac{\partial \Delta C_{pL}}{\partial T}\right)_p = \left(\frac{\partial^2 \Delta H_d}{\partial T^2}\right)_p \xi_e + 2\left(\frac{\partial \Delta H_d}{\partial T}\right)_p \left(\frac{\partial \xi_e}{\partial T}\right)_p + \Delta H_d \left(\frac{\partial^2 \xi_e}{\partial T^2}\right)_p \quad (16)$$

urther analysis of the model requires to specify the analytical expression of the Gibbs energy difference between the 2 states. As it is classically done in CALPHAD modelling, ΔG_d is expanded under the form:

$$\Delta G_d = \Delta H_d - T\Delta S_d = A + BT + CT\ln T + dT^2 \ldots \quad (17)$$

The review of the literature presented in the next section shows that, in practice, the expansion is never continued beyond the third term and in many cases is limited to the first 2 terms. Hence, we have in the most complex case:

$$\Delta G_d = \Delta H_d - T\Delta S_d = A + BT + CT\ln T \quad (18)$$

$$\Delta S_d = -B - C(1 + \ln T) \quad (19)$$

$$\Delta H_d = A - CT \quad (20)$$

$$\Delta C_{pd} = -C \quad (21)$$

We will now study in more depth 3 cases of increasing complexity.

Case 1

The first and simplest case corresponds to $B = C = 0$ then:

$$\Delta G_d = \Delta H_d = A > 0 \text{ and } \Delta S_d = 0 \quad (22)$$

Note that this case is in practice of little interest for the description of a real liquid; however it helps to understand the behavior of the model. The enthalpy of the excited state B is by definition higher than that of the ground state A and hence only positive values of the A parameter are allowed.

The fraction of excited units given by equation (9) is restricted to evolve between $\xi_e = 0$ at 0 K and $\xi_e = 0.5$ in the high $T \to \infty$ temperature limit, where the ground and excited energy levels are equally populated because it is a configuration that maximizes the entropy of mixing.

As ΔH_d does not depend on temperature, the heat capacity difference reduces to:

$$\Delta C_{pL} = \Delta H_d \left(\frac{\partial \xi_e}{\partial T}\right)_p \quad (23)$$

Injecting (13) in (23), the well-known analytical expression (e.g. eq.(3) of [37] or eq. (6) of [38]) of the "Schottky anomaly" heat capacity hump (black solid curve in Figure 1) is obtained:

$$\Delta C_{pL} = R\left(\frac{\Delta H_d}{RT}\right)^2 \xi_e(1 - \xi_e) \quad (24)$$

The temperature T_{max} of the maximum of the configurational heat-capacity hump can be calculated by applying the condition:

$$\left(\frac{\partial \Delta C_{pL}}{\partial T}\right)_p = 0 \quad (25)$$

Using eq. (23):

$$\left(\frac{\partial \Delta C_{pL}}{\partial T}\right)_p = \Delta H_d \left(\frac{\partial^2 \xi_e}{\partial T^2}\right)_p = 0 \tag{26}$$

After some calculations, it is found that (see Prigogine & Defay [39] page 298):

$$\frac{\Delta H_d}{2RT_{max}} \tanh \frac{\Delta H_d}{2RT_{max}} = 1 \tag{27}$$

This equation can be solved numerically, the positive root is:

$$\frac{\Delta H_d}{2RT_{max}} \approx 1.19968 \ldots \text{or} \ \frac{RT_{max}}{\Delta H_d} \approx \frac{1}{2 \times 1.19968} \approx 0.41677 \ldots \tag{28}$$

Injecting eq. (27) in (24) and after some simplifications, the heat capacity maximum reads:

$$\Delta C_{pL,max} = \frac{R}{4}\left(\left(\frac{\Delta H_d}{RT_{max}}\right)^2 - 4\right) \approx 0.44\, R \tag{29}$$

This equation can also been found in the book of Gasser & Richards [40] (page 87).

It is also interesting to note that, due to equation (26), the maximum value of the heat capacity coincides with the inflection point of the excitation profile hence we have:

$$T_{inf} = T_{max} \tag{30}$$

This coincidence is highlighted by the vertical black dotted line in Figure 1.

As ΔH_d does not depend on temperature, equation (15) reduces to:

$$\xi_{e,inf} = \frac{1}{2} - \frac{RT_{inf}}{\Delta H_d} \tag{31}$$

By directly injecting (31) in (24), we can re-demonstrate more easily equation (29).

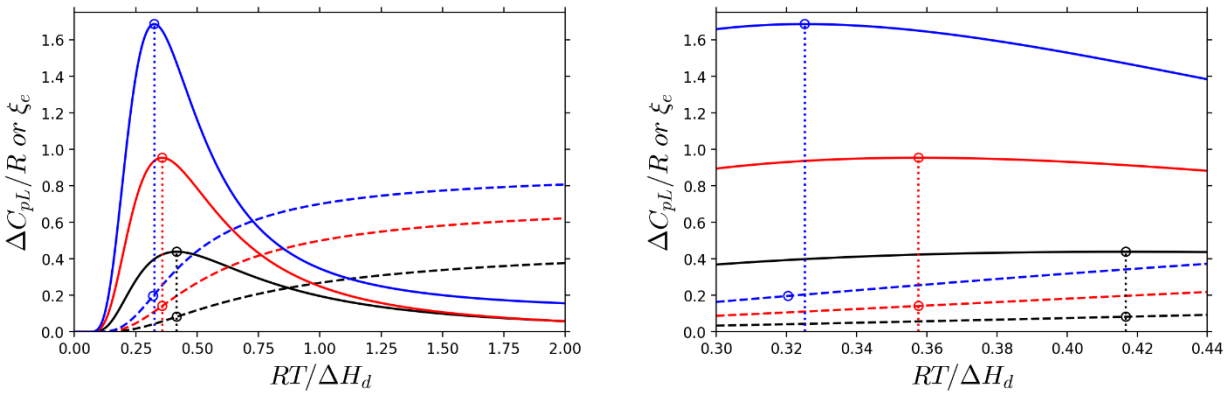

a) for $0 < RT/\Delta H_d < 2$

b) enlarged view in the temperature region of the heat capacity maximum and inflexion of the excitation profile

Figure 1. Reduced heat capacity hump ($\Delta C_{pL}/R$, *solid lines*) *and excitation profile* (ξ_e, *dashed lines*) *of the ideal 2-state model as a function of dimensionless temperature* $RT/\Delta H_d$ *for* $\Delta G_d = A$ *(black curves),* $\Delta G_d = A - RT$ *(red curves) and* $\Delta G_d = A - RT + CTlnT$ *(blue curves), with* $A = 10000\ J\ mol^{-1}$ *and* $C = -1\ J\ mol^{-1}\ K^{-1}$. *The vertical dotted lines highlight the coincidence of the maximum heat capacity and the inflection point of the excitation profile, which both occur at the same temperature for the black and red curves, whereas these two points do not coincide for the blue curve.*

Increasing the positive value of the enthalpy parameter A shifts the peak of the heat capacity (and the rise of the excitation profile) towards higher temperatures and also enlarges the peak width (Figure 2).

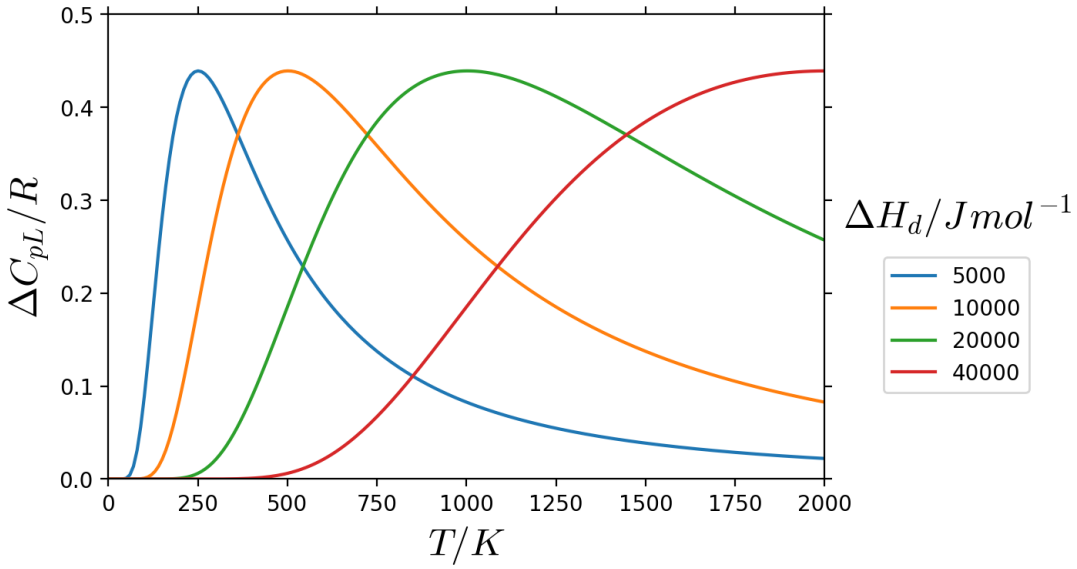

Figure 2. Reduced heat capacity hump ($\Delta C_{pL}/R$) *of the ideal 2-state model for various values of* $\Delta G_d = A = \Delta H_d$ *as a function of temperature. These curves all collapse into a single master-curve shown in Figure 1 when plotted in dimensionless temperature.*

This analysis shows that the use of a single enthalpy parameter A does not offer much flexibility in fitting the heat capacity data as only the position and shape of the heat capacity peak can be changed, although not independently, but the height of the peak is fixed, as is the high temperature limit ($\xi_e = 0.5$) of the excitation profile. For the same reason, and because of eq. (11), the enthalpy change is restricted to obey the inequality $\Delta H_L < 0.5\Delta H_d$. It is concluded that, for practical use of the ideal 2-state model, more terms are needed in the expansion of eq. (17).

Case 2

Greater flexibility is indeed obtained when a non-zero entropy parameter B is used in eq. (17). We then have:

$$\Delta G_d = A + BT, \;\; \Delta H_d = A > 0 \;\text{ and }\; \Delta S_d = -B > 0 \tag{32}$$

Like the enthalpy, the entropy of the excited state B is also assumed to be higher than that of the ground state A. This physical constraint requires the B parameter to be negative.

The high temperature limit of ξ_e becomes:

$$\lim_{T\to\infty} \xi_e = \frac{1}{1 + exp\left(\frac{B}{R}\right)} \tag{33}$$

Then if, for example, $B = -R$, $\lim_{T\to\infty} \xi_e \approx 0.731$ and if $B = -2R$, $\lim_{T\to\infty} \xi_e \approx 0.881$. The conclusion is that the B parameter allows to increase the high temperature limit of ξ_e.

Applying again condition (25) to find the temperature of the heat capacity maximum, the following equation is obtained:

$$\frac{\Delta H_d}{2RT_{max}} \frac{exp\frac{\Delta H_d}{RT_{max}} - exp\frac{\Delta S_d}{R}}{exp\frac{\Delta H_d}{RT_{max}} + exp\frac{\Delta S_d}{R}} = 2 \tag{34}$$

If $\Delta S_d = R$, the "communal entropy" value frequently used to parametrize the model (see Table 1), eq. (34) becomes:

$$\frac{\Delta H_d}{2RT_{max}} \frac{exp\frac{\Delta H_d}{RT_{max}} - e}{exp\frac{\Delta H_d}{RT_{max}} + e} = 2 \tag{35}$$

In which e is the Euler number. This equation can be solved numerically, the positive root is:

$$\frac{\Delta H_d}{RT_{max}} \approx 2.79597 \ldots \text{or } \frac{RT_{max}}{\Delta H_d} \approx 0.35766 \ldots \tag{36}$$

Again, as ΔH_d does not depend on temperature, eq. (23), (26) and (30) hold and the heat capacity maximum coincides with the inflexion point of the excitation profile. By substituting the root value given by eq. (36) in eq. (29) the heat capacity maximum is:

$$\Delta C_{pL,max} \approx 0.95\, R \tag{37}$$

Comparatively to case 1, Figure 1b shows that, for case 2, the heat capacity maximum is increased (e.g. from $\approx 0.44R$ up to $\approx 0.95R$ if $B = -R$) and the excitation profile has a steeper slope, hence its inflexion point is shifted to lower temperatures.

Case 3

We now consider the full 3-term expression given by eq. (18). This modeling solution is quite often selected by users of the model as can be checked in Table 1. Both positive and negative values of the C heat capacity parameter are adopted.

First, it is important to check the asymptotic behavior of the 2-state model when the C parameter has a non-zero value.

The high temperature limit of ξ_e becomes:

$$\lim_{T\to\infty} \xi_e = \lim_{T\to\infty} \frac{1}{1 + T^{\left(\frac{C}{R}\right)}} \tag{38}$$

The above expression shows that if $C < 0$, the fraction of excited units tends towards 1 at high temperature but if $C > 0$, this fraction tends to zero. Hence, this last choice does not seem to be physically reasonable, considering that the excited state is expected to be the most populated at high temperature.

Figure 1 shows that, compared to case 2, for case 3, the heat capacity maximum is again increased and the excitation profile has a steeper slope and its inflexion point is shifted to lower temperatures however, the maximum heat capacity and the inflexion point of the excitation profile no longer coincide (see Figure 1b). This is because the second term on the right side of equation (16) has a non-zero value. The order of magnitude of the offset remains small in the numerical application shown in Figure 1.

In the high $T \to \infty$ temperature limit the excitation profile $\xi_e \to 1$, the second term on the right side of eq. (12) vanishes and the heat capacity $\Delta C_{pL} \to -C$.

As a final conclusion to this section, we would like to point out that in all three cases studied, the shape of the excitation profile remains sigmoidal with a moderate slope, the main change being the limiting value of ξ_e at high temperature.

2 Parametrization of the ideal 2-state model

To implement the model, the first task consists in assessing the Gibbs energy, denoted G_A°, of the 100%A liquid, considered as the ground state, and the second tasks in assessing the Gibbs energy difference, denoted ΔG_d, between the ground-A and excited-B states:

$$\Delta G_d = G_B^\circ - G_A^\circ \tag{39}$$

Few words about the first task. The G_A° function represents a "base line" or "background" contribution to the Gibbs energy function of the liquid. The choice of this function has profound effect on the subsequent choice of the ΔG_d parameters. Three modelling methodologies have been identified from reading of the literature.

The first one is what could be called a "Lattice Stability" approach. G_A° is in this case defined by a difference from the Gibbs energy of the crystalline phase, acting as a reference state on which experimental and calculated thermodynamic data are available. In this approach, e.g. [3] [6], the harmonic, Einstein-like ($GEinstein$), contributions to the thermodynamic functions of the 100% A liquid and that of the crystal are the same:

$$G_{100\%A} = GEinstein_{cryst} + a + bT + dT^2 + \cdots \tag{40}$$

Ågren et al. [7] [14], rather selected the following expression:

$$G_{100\%A} = G_{cryst} + a + bT + cTlnT + dT^2 \text{ with } b = -R \tag{41}$$

In the second one, the 100% A liquid has its own, estimated, harmonic contribution different from that of the crystal e.g. [5]. A single Einstein function is used in this approach because of the lack of experimental data to fit the parameters of any additional Einstein function. The Gibbs energy is written as:

$$G_{100\%A} = GEinstein_{100\%A} + a + bT + dT^2 + \cdots \tag{42}$$

In the third one, well adapted for glass forming substances such as SiO_2 [23], GeO_2 [24] or B_2O_3 [21], experimental data of the glass are used to define the functions of the 100% A liquid:

$$G_{100\%A} = GEinstein_{glass} + a + bT + dT^2 + \cdots \tag{43}$$

Despite the pragmatic nature of CALPHAD modelling, there are theoretical arguments for the adoption of specific parametrization guidelines. Obviously, if the modeling extends down to 0 K, c in eq. (41) should have a zero value because the heat capacity must vanish at zero temperature. Less obviously, b should also have a zero value because the residual entropy of a metastable liquid in internal equilibrium at 0 K should be zero. Complementary information on this topic can be found in our previous work [21]. The effect of adopting this second guideline on the calculated heat capacity and entropy evolutions is particularly well illustrated by figure 2 of reference [20].

Our analysis is then focused on the second parametrization task which consists in fitting the ΔG_d contribution. We present in Table 1, a list of chemical elements that have been described using the ideal 2-state model and the corresponding values of the parameters A, B and C in the ΔG_d expansion. These parameters are tuned to reproduce the melting temperature and melting enthalpy, and, when available, heat capacity and heat increment data of the liquid phase. This element list, perhaps not exhaustive, is at least representative of the work that has been done in this area over the last 20 years. Al, Au and Sn have been described twice and C and Fe three times. The excitation profiles of all these descriptions are compared graphically in Figure 3.

The A, B and C parameter values in this table remain difficult to rationalize without a detailed analysis in each case. It is worth adding that these values are not independent from the modeling options adopted to describe the "100%A liquid background contribution" to the Gibbs energy of the liquid phase as explained above. Some global trends can nevertheless be highlighted.

The key parameters are A and B, as explained in previous section, and in 10 descriptions, only these two parameters are indeed used. A third parameter C is added in the remaining 11 descriptions.

Figure 3 shows that when small values of A are used, the excitation profile resembles a step rather than a sigmoid.

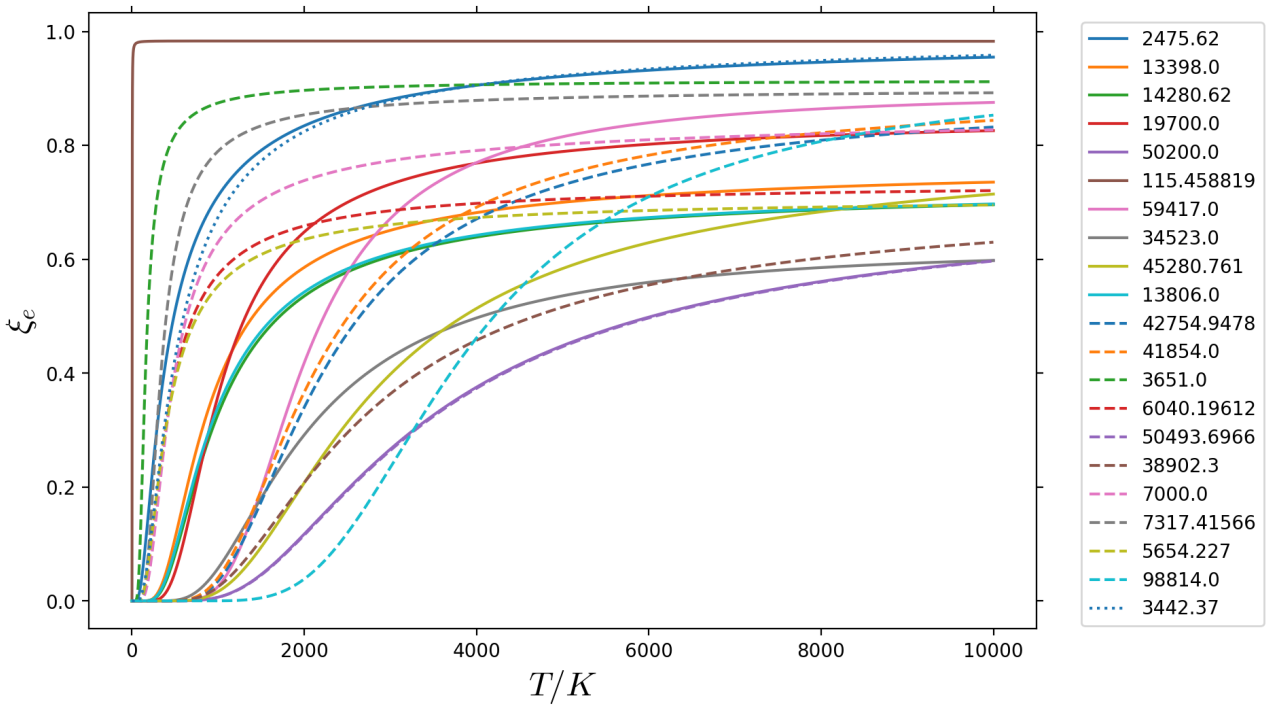

Figure 3. Excitation profiles for the 21 descriptions listed in Table 1. For each curve, the coefficient A *used in the* ΔG_d *expansion is used as the curve label and the corresponding values of the parameters* B *and* C *can be found in Table 1.*

Three descriptions are considered "atypical" and they are labelled with a star in Table 1 and Figure 4. Carbon has been described three times by Selleby and coworkers. In the initial description [8], the A parameter is very close to zero but was amended to more usual values in later works [5] [20] by the same group. However, the C heat capacity parameter is positive in the three successive carbon descriptions. Because of eq. (38), this choice is questionable. However, this criticism remains rhetorical, as the decrease in ξ_e with increasing temperature, predicted on the basis of eq. (38), occurs in these descriptions only at extremely high temperatures, well above the temperature range relevant to CALPHAD modeling.

In the study of Dinsdale et al. [4], large and positive values of the entropic B parameter were chosen for Al and Zn. Note that a similar choice was also made in the modeling of CaO by Deffrenes et al. [22]. This modeling choice implies that the entropy of the excited state is lower than that of the ground state and appears somewhat contradictory to the common interpretation of the ground state being "solid-like" and excited state being "liquid-like" or "gas-like" and to the communal entropy concept. It is worth noting that large negative C values are systematically adopted to counterbalance the effect of large positive B values.

Table 1. Parametrization of the Gibbs energy difference of the ideal 2-state model for a list of chemical elements. Numerical values of the A, B and C parameters are taken from the original articles, melting temperature and enthalpy of the elements are from SGTE [41].

Ref.	Element	T_m	$\Delta_m H$	$\Delta_m S$	A	B	C	$\frac{A}{\Delta_m H}$	$-\frac{B}{\Delta_m S}$
		K	$J\ mol^{-1}$	$J\ (mol\ K)^{-1}$	$J\ mol^{-1}$	$J\ (mol\ K)^{-1}$	$J\ (mol\ K)^{-1}$		
[4](★)	Al	933.47	10711.04	11.474	2475.62	37.10227	-6.81347	0.23	-3.23
[5]					13398	-8.314	-0.16597	1.25	0.72
[3]	Au	1337.33	12552	9.386	14280.62	-8.314	0	1.14	0.89
[6]					19700	-14.917	0	1.57	1.59
[7]	B	2348	50200	21.380	50200	-8.314	0	1	0.39
[8](★)					115.458819	-34.9955761	0.141746933	0.001	1.42
[5]	C	4765.3	117369	24.630	59417	-49.61	2.9806	0.51	2.01
[20]					34523	-24.6	1.93765	0.29	1.00
[9]	Co	1768	16200	9.163	45280.761	-8.314	-0.417144850	2.80	0.91
[7]					13806	-8.314	0	1	1.09
[10]	Fe	1811	13806	7.623	42754.9478	-7.624	-1.08230446	3.10	1.00
[11]					41854	-7.626	-1.150476	3.03	1.00
[3]	Ga	302.91	5589.82	18.454	3651	-19.7942	0	0.65	1.07
[12]	In	429.75	3283	7.639	6040.19612	-8.48211292	0	1.84	1.11
[13]	Mn	1519	12908.94	8.498	50493.6966	-8.314	0	3.91	0.98
[14]	Nb	2750	30000	10.909	38902.3	-8.314	0	1.30	0.76
[15]	Pb	600.612	4773.94	7.948	7000	-4.518	-1	1.47	0.57
[16]	Sn	505.078	7029.12	13.917	7317.41566	-18.3219791	0	1.04	1.32
[17]					5654.227	-7.4269650	0	0.80	0.53
[18]	W	3695	52313.69	14.158	98814	-13.653	-1.178678	1.89	0.96
[4](★)	Zn	692.68	7322	10.571	3442.37	41.34521	-7.35647	0.47	-3.91

(★) *Description is considered atypical (see text for explanation).*

Excluding the three atypical descriptions, the value of parameter A globally increases as the melting point rises (Figure 4) however, the trend is obscured by the considerable dispersion affecting the values above 1500 K because for high-melting elements, for which heat capacity is very difficult to measure, data is very scarce or largely missing and optimization is only weakly constrained. Such an increase of parameter A is needed if one considers that i) the parameter A governs the position of the heat capacity hump (see Figure 2) and ii) this hump must be located within a certain temperature range below the melting temperature and must therefore be moved to higher temperatures when higher melting elements are considered. It is also interesting to note that the increasing trend is quite clear for the low melting elements and even appears linear (cf. dashed line Figure 4). For these elements, experimental values of the heat capacity of the liquid phase are available, sometimes both below and above the melting point, and well constrain the optimization.

The $-B/\Delta_m S$ average value calculated from all studies listed in Table 1 is 1 with a standard deviation of 0.4 meaning that the entropic parameter is rather close to the melting entropy. In some cases $B = -R$, the so-called communal entropy value is selected but in most of these cases the melting entropy is itself not far from R. This is because the Richard's rule is quite well obeyed for many elements as can be checked from figure 12.2 page 194 of Grimvall's book [42].

As a further comment, for glass forming substances, the configurational entropy of the liquid at the melting temperature can be quite reliably estimated from the thermodynamic data of the glass and the equilibrium liquid. It was shown in [21] that there is a constraint between the A and B parameters and that they cannot be considered as two independent parameters; only one of them can be freely optimized. The optimization process was found to be somewhat over-constrained in the B_2O_3 test-case studied in

[21].

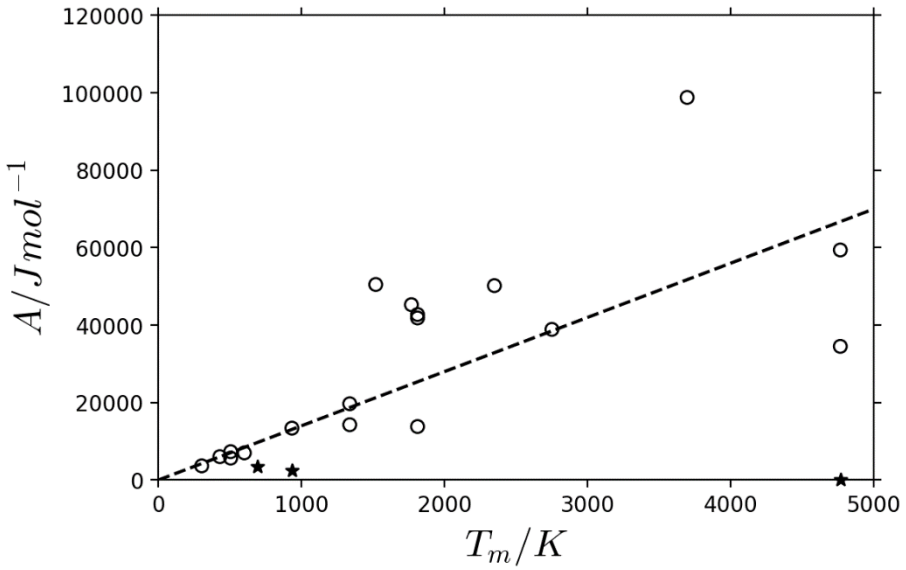

Figure 4. "A-parameter" values as a function of the melting temperature T_m for a list of 14 chemical elements. Data extracted from 21 literature descriptions (see Table 1 for details). The dashed line is a linear fit based on the low melting points $(T < 1500\ K)$ *element data, the regression line is* $(A/J\ mol^{-1}) \approx 14(T/K)$. *Star symbols* (★) *correspond to atypical parametrizations that cannot be analyzed with the same rationale as other works* (○) *(see text for explanation).*

It is tempting to add a third C parameter in the ΔG_d expansion eq. (17). It was shown in former section that positive C values are difficult to justify. A personal view, not necessarily shared by all users of the 2-state model in the CALPHAD literature, is to keep the value of the third C heat-capacity parameter at zero. The justification as explained in [21] being that, when the 2-state model is coupled to a relaxation kinetic model to simulate the glass transition, adopting a zero value for C guarantees that the heat capacity of the liquid reduces to the heat capacity of the 100%A phase at temperatures lower than the glass transition temperature, where the configurational contributions to the thermodynamic functions are frozen in. However, we recognize that describing the kinetics of the glass transition by coupling a thermodynamic model with a relaxation law is not the objective of most CALPHAD work.

The conclusions of this empirical analysis of the ideal 2-state model are i) more parameters maybe needed in some cases to increase the fitting ability of the model, ii) adding parameters in the expansion of the Gibbs energy difference between the 2 states might not be the best choice. More fundamental reasons to enrich the ideal 2-state model can been found in glass research literature and are developed in the next section.

3 Limits of the ideal 2-state model

We can classify the criticisms in two categories namely i) the limited ability of the ideal model to fit experimental heat capacity curves and ii) the very simple phenomenology of the ideal 2-state model which basically only describes a sigmoid increase of the fraction of excited units with temperature (see Figure 5, $w = 0$ curve), not allowing any other behavior.

In the first category, Nemilov (page 34 of [43]) mentions that the configurational heat capacity curve calculated by the Schottky function "does not render the shape of the ΔC_p experimental curves over a wide temperature range correctly". Another physical interpretation of the two levels of the model in covalent network-forming liquids is that the ground level represents an intact bond while the excited level represents a broken bond [44]. In the ideal version of the model, the energy needed for breaking of a bond is hence totally independent of the potential adjacency of broken bonds so there is no cooperative character. Angell & Rao [44] and Goldstein [45] early recognized that introducing a degree of

cooperativity could in some cases improve the ability of the model to fit the experimental data. Moreover, Angell (page 6470 of [46]) noticed for selenium a "disagreement of the experimental heat capacity with that of the simple (paradox free) excitation model".

In the second category, it is now quite firmly established [47] [48] [49] [50] [51] [52] that, when the $p-T$ plane is explored, Liquid-Liquid (LL) phase separation (liquid polymorphism) can occur in various types of pure substances and that this kind of phase transition might explain "amorphous polymorphism" (also called "poly-amorphism", meaning the existence of two glasses having the same composition but differing densities and entropies), pressure induced amorphization [53] and the Fragile To Strong (FTS) transition observed in a growing number of glasses, as recently reviewed by Lucas [54], including metallic glasses [55]. By its very construction, the ideal 2-state model is unable to describe any phase separation phenomenon.

By analogy with the behavior of binary solutions, the simplest increase in complexity one can imagine to depict a LL phase separation is to move from an ideal solution model to a regular solution model. This type of 2-state model has been only superficially reviewed in [21]. Among the numerous works published in the field since the 1960s, it is particularly worth recalling the "2-species model" of Rapoport[1] [56] [57], the "pseudo-regular binary solution model" of Ponyatovsky et al. [53] [58] [59] [60], the "2-species non-ideal model" of Moynihan [61] and "the cooperative bond-lattice model" of Angell, Moynihan et al. [37] [62] or the "2-state model with cooperativity" of Tanaka [63]. All these models refer in fact to the same binary regular solution formalism and have much in common with the earlier and more complex model of Strässler & Kittel [64], in which the degeneracies of the two energy levels are taken into account.

In their attempts to model the thermodynamic properties of supercooled water, Bertrand & Anisimov [65] and Holten & Anisimov [66] initially used a 2-state "athermal solution model" having a zero enthalpy of mixing but a non-ideal entropy of mixing. Later studies [67] [68] of the same group emphasized the use of a new and more sophisticated 2-state model, having a mixed character, in which both athermal and regular solution contributions are combined through a weighed sum. However, it was concluded in both articles that the behavior of supercooled water could be successfully described by keeping only the regular contribution.

For the sake of completeness, it is worth mentioning an alternative and final way of enriching the ideal two-state model that has been implemented by Moynihan & Angell [69]. They introduce into the model a third adjustable parameter, denoted n, representing the "number of moles of excitable states or degrees of freedom per molecule or formula units". In the list of 17 liquids studied in their paper, this parameter has integer values ranging from 1 for selenium to 7 for glycerol and appears as a multiplicative factor in the expressions for entropy and heat capacity. This concept of a "bead" which is the excitable subunit of the molecule, n being the number of beads, has its origins in the polymer literature, particularly in the work of Wunderlich [70]. However, this number is not always univocally defined and, for a given substance, may have different values depending on the author (e.g. Table I of [71]). In a more recent publication, Klein & Angell [72] page 118 recognize that the definition of the bead is "very uncertain and leaves much room for subjective adjustment". This concept is not explored further in the present work.

This concise review of the literature shows that adding a regular solution interaction term to the ideal two-state model is a very simple development, as only one parameter is added to the model, which allows many characteristics of glass-forming unary liquids to be described.

To be more convincing, we now propose a deeper analysis of the regular 2-state model.

[1] Rapoport wanted to explain the melting curve maxima at high pressures in substances such as liquid Cs and Te and did not specifically address the case of LL phase separation.

4 Formalism and phase diagram of the regular 2-state model

The Gibbs energy of the regular A-B liquid solution reads:

$$G_L = \xi_A G_A^\circ + \xi_B G_B^\circ + RT(\xi_A ln\xi_A + \xi_B ln\xi_B) + w\xi_A\xi_B \tag{44}$$

By keeping a single $\xi_B = 1 - \xi_A = \xi$ internal compositional variable, the Gibbs energy is rewritten:

$$G_L = (1-\xi)G_A^\circ + \xi G_B^\circ + RT((1-\xi)\ln(1-\xi) + \xi\ln\xi) + w\xi(1-\xi) \tag{45}$$

The internal equilibrium condition is obtained by taking:

$$\left(\frac{\partial G_L}{\partial \xi}\right)_{\xi=\xi_e} = 0 \tag{46}$$

Using (45), we get:

$$(G_B^\circ - G_A^\circ) + RT(\ln\xi_e - \ln(1-\xi_e)) + w(1-2\xi_e) = 0 \tag{47}$$

We introduce the Gibbs energy difference ΔG_d between the two states and express it as the sum of its enthalpic and entropic contributions:

$$\Delta G_d = G_B^\circ - G_A^\circ = \Delta H_d - T\Delta S_d \tag{48}$$

The configurational Gibbs energy of the solution (44) now reads:

$$\Delta G_L = G_L - G_A^\circ = \xi\Delta G_d + RT((1-\xi)\ln(1-\xi) + \xi\ln\xi) + w\xi(1-\xi) \tag{49}$$

And the internal equilibrium condition (47) then becomes:

$$\Delta G_d + RT\ln\frac{\xi_e}{1-\xi_e} + w(1-2\xi_e) = 0 \tag{50}$$

We are now interested in finding the equilibrium state.

In contrast to the case of the ideal 2-state model, a simple $\xi(T)$ expression such as eq.(6) cannot be obtained from eq. (50) and this last equation, possibly having more than one solution, has to be solved numerically.

However, an analytical solution of eq. (50) can be obtained if the inverse problem is considered. We then define ξ as the independent variable and an expression $T(\xi)$ is sought. Injecting eq. (48) in eq. (50) and rearranging terms, we get:

$$T = \frac{\Delta H_d + w(1-2\xi_e)}{\Delta S_d - R\ln\frac{\xi_e}{1-\xi_e}} \tag{51}$$

Eq. (51) is plotted for fixed values of ΔH_d and ΔS_d and several values of the interaction parameter w in Figure 5, selecting T as the abscissa and ξ_e as the ordinate.

From eq. (51), it is seen that:

$$T(\xi_e = 1/2) = \Delta H_d/\Delta S_d \tag{52}$$

Hence, whatever the value of w, all curves will intersect at the point $(\Delta H_d/\Delta S_d;\ 1/2)$.

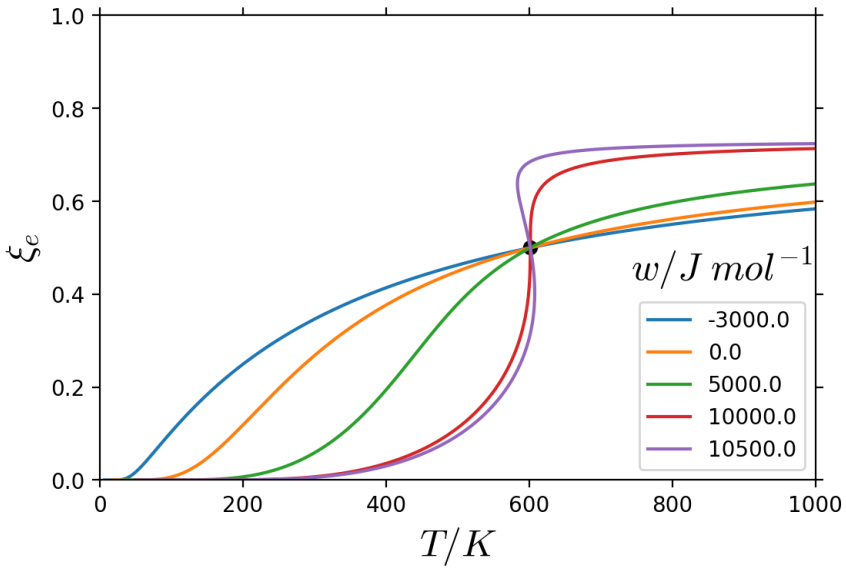

Figure 5. Molar fraction of excited-B structural units vs. temperature under internal equilibrium conditions for $\Delta H_d = 5000\ J\ mol^{-1}$, $\Delta S_d = R$ *and various values of* $w\ /\ J\ mol^{-1}$. *All curves intersect at* $(T = 5000/R \approx 601.4\ K; \xi = 0.5)$. *The critical value of the interaction parameter is:* $w_c = 10000\ J\ mol^{-1}$ *corresponds to the red curve with a vertical tangent at the critical point (black dot).*

The case $w = 0$ corresponds to the ideal 2-state model. As w is increased from -3000 to $+10500\ J\ mol^{-1}$, the shape of $\xi(T)$ gradually changes from a sigmoid of increasing steepness to an S-shaped curve when the interaction parameter w becomes greater than its critical value w_c. It is well known (e.g. [73] page 82) that, for a binary regular solution, the critical point corresponds to $\xi_e = 1/2$ and a critical temperature T_c which only depends on the value of the interaction parameter:

$$T_c = \frac{w}{2R} \tag{53}$$

Combining equations (52) and (53), the critical value of the interaction parameter for fixed values of ΔH_d and ΔS_d is obtained:

$$w_c = 2R\frac{\Delta H_d}{\Delta S_d} \tag{54}$$

For $w > w_c$ (e.g. for $w = 10500\ J\ mol^{-1}$ in Figure 5, $\xi_e(T)$ is no longer a function, the S-shape is the signature of the development of instability. The behavior becomes similar to the famous van der Waals EOS of gases and liquids. Because of the repulsive interaction between dissimilar units, the liquid will then unmix into an A-rich liquid and a B-rich liquid.

Let us now establish the phase diagram of the model. As temperature is changed and depending on the values of the ΔH_d, ΔS_d and w parameters of the model, the shape of the $\Delta G_L(\xi)$ curve evolves and eq. (50) might have more than one solution. The equilibrium value of ξ will be obtained by searching for the deepest minimum of the Gibbs energy function of the solution.

As an example, the $\Delta G_L(\xi)$ is plotted at different temperatures in Figure 6. At each temperature, the equilibrium state corresponds to the deepest minimum of the Gibbs energy curve. At low temperatures, the deepest minimum is on the A-rich side ($\xi_e < 0.5$), while, at high temperatures, it is on the B-rich side ($\xi_e > 0.5$). The condition of coexistence of the two liquids corresponds to the situation where $\Delta G_L(\xi)$ has two minima of equal depth. For given values of ΔH_d and ΔS_d, this condition is fulfilled at the temperature T_{LL} for which:

$$\Delta G_d(T_{LL}) = 0 \tag{55}$$

implying that $T_{LL} = \Delta H_\mathrm{d}/\Delta S_\mathrm{d}$.

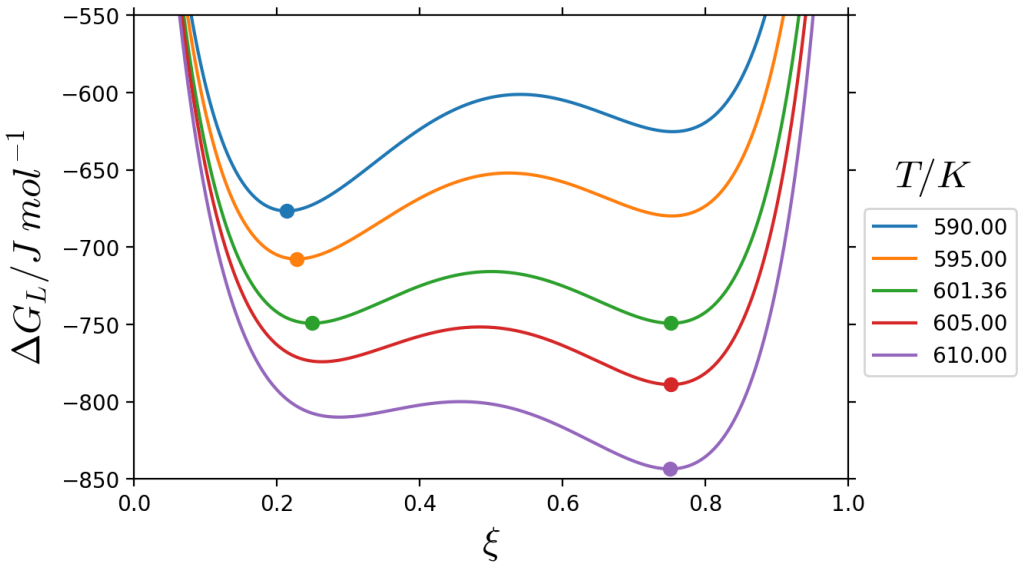

Figure 6. Gibbs energy of the liquid ΔG_L *vs.* ξ *at various temperatures for* $\Delta H_d = 5000\ J\ mol^{-1}$, $\Delta S_d = R$ *and* $w = 11000\ J\ mol^{-1}$. *The dots corresponds to equilibrium compositions which are minima of the Gibbs energy curves. At* $(T_{LL} = \Delta H_d/\Delta S_d \approx 601.36\ K)$, *the Gibbs energy curve has two minima of equal depth. These two minima give the composition of the 2 liquids in equilibrium. At lower T, the liquid is A-rich and at higher T the liquid is B-rich.*

By taking $\Delta G_d = 0$ in the internal equilibrium condition (50) and after rearranging terms, the equation of the binodal or miscibility gap curve reads:

$$T = \frac{w(2\xi_e - 1)}{R\ln\left(\frac{\xi_e}{1-\xi_e}\right)} \tag{56}$$

The spinodal curve is defined using the stability limit condition:

$$\left(\frac{\partial^2 G_L}{\partial \xi^2}\right) = 0 \tag{57}$$

Hence, the equation of the spinodal curve is simply obtained by taking the derivative of eq. (50) with respect to ξ, yielding:

$$T = \frac{2w}{R}\xi(1-\xi) \tag{58}$$

Let-us define the dimensionless temperature:

$$T^* = T/T_c \tag{59}$$

The dimensionless form of eq. (56) reads:

$$T^* = \frac{2(2\xi_e - 1)}{\ln\left(\frac{\xi_e}{1-\xi_e}\right)} \tag{60}$$

And the dimensionless form of eq. (58) reads:

$$T^* = 4\xi(1-\xi) \tag{61}$$

Equation (61) shows that all spinodal curves merge, regardless of the value of the interaction parameter, when plotted against the dimensionless temperature. Hence, in dimensionless variables, it is seen that the regular 2-state model obeys a sort of "law of corresponding states" and has a universal temperature-composition phase diagram plotted in Figure 7.

The internal equilibrium condition (51) is similarly put under dimensionless form:

$$T^* = 2\frac{\Delta H_d/w + (1-2\xi_e)}{\Delta S_d/R - \ln\frac{\xi_e}{1-\xi_e}} \tag{62}$$

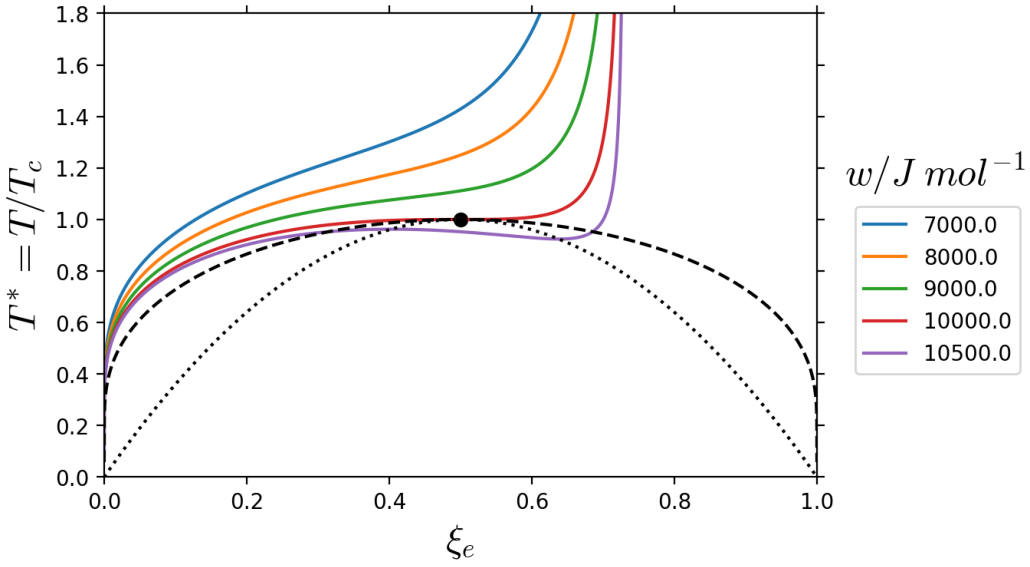

Figure 7. Universal temperature-composition phase diagram of the regular 2-state model. The dashed line is the miscibility gap and the dotted line is the spinodal curve. The equilibrium fractions of excited-B units calculated with eq. (62) for $\Delta H_d = 5000\ J\ mol^{-1}$, $\Delta S_d = R$ *and various values of* w *are superimposed on the diagram. The red curve, which corresponds to the critical value of* w*, is tangent to the miscibility gap at the critical point (black dot).*

If the spinodal curve is to be plotted as a function of temperature, the following quadratic equation must be solved:

$$4\xi^2 - 4\xi + T^* = 0 \tag{63}$$

Of which the two solutions for $T^* \leq 1$ are the upper and lower branches of the spinodal curve:

$$\xi_{\substack{\text{up}\\\text{low}}} = \frac{1 \pm \sqrt{1-T^*}}{2} \tag{64}$$

5 Thermodynamic functions of the regular 2-state model

The analytical expressions of the configurational thermodynamic functions of the liquid at ambient pressure are now established.

By derivation of the Gibbs energy (eq. (49)) with respect to temperature, and using the internal equilibrium condition (50), the entropy difference of the liquid reads:

$$\begin{aligned}\Delta S_L = S_L - S_A^\circ &= -\left(\frac{\partial \Delta G_L}{\partial T}\right)_p \\ &= \xi_e \Delta S_d - R((1-\xi_e)\ln(1-\xi_e) + \xi_e \ln\xi_e) - \left(\frac{\partial w}{\partial T}\right)_p \xi_e(1-\xi_e)\end{aligned} \tag{65}$$

If w does not depend on temperature, the last term is cancelled and the entropy of the ideal solution is recovered:

$$\Delta S_L = \xi_e \Delta S_d - R((1-\xi_e)\ln(1-\xi_e) + \xi_e \ln\xi_e) \tag{66}$$

The liquid enthalpy is easily calculated using the classical relation:

$$\Delta H_L = \Delta G_L + T\Delta S_L \tag{67}$$

With eqs. (49) and (65) :

$$\Delta H_L = H_L - H_A^\circ = \xi_e \Delta H_d + \left(w - T\left(\frac{\partial w}{\partial T}\right)_p\right)\xi_e(1-\xi_e) \tag{68}$$

Again, if w does not depend on temperature, the last term is cancelled:

$$\Delta H_L = \xi_e \Delta H_d + w\xi_e(1-\xi_e) \tag{69}$$

By derivation of the internal equilibrium (50) condition with respect to temperature, the expression for the derivative of the internal variable with respect to temperature is deduced:

$$\left(\frac{\partial \xi_e}{\partial T}\right)_p = \frac{\Delta S_d - R\ln\frac{\xi_e}{1-\xi_e} - \left(\frac{\partial w}{\partial T}\right)_p (1-2\xi_e)}{\left(\frac{RT}{\xi_e(1-\xi_e)} - 2w\right)} \tag{70}$$

The configurational heat capacity can now be calculated by differentiating the enthalpy (eq. (68)) with respect to temperature and substituting eq. (70) to simplify the expression. It reads:

$$\Delta C_{pL} = C_{pL} - C_{pA}^\circ = \left(\frac{\partial \Delta H_L}{\partial T}\right)_p = \xi_e\left(\frac{\partial \Delta H_d}{\partial T}\right)_p - T\left(\frac{\partial^2 w}{\partial T^2}\right)_p \xi_e(1-\xi_e) + \frac{\Delta S_d - R\ln\frac{\xi_e}{1-\xi_e} - \left(\frac{\partial w}{\partial T}\right)_p (1-2\xi_e)}{\left(\frac{RT}{\xi_e(1-\xi_e)} - 2w\right)}\left(\Delta H_d + w(1-2\xi_e) - T\left(\frac{\partial w}{\partial T}\right)_p (1-2\xi_e)\right) \tag{71}$$

If w is independent of temperature, eq. (71) simplifies to:

$$\Delta C_{pL} = \xi_e\left(\frac{\partial \Delta H_d}{\partial T}\right)_p + \frac{\Delta S_d - R\ln\frac{\xi_e}{1-\xi_e}}{\left(\frac{RT}{\xi_e(1-\xi_e)} - 2w\right)}(\Delta H_d + w(1-2\xi_e)) \tag{72}$$

If ΔH_d is also independent of temperature, equation (72) further simplifies to:

$$\Delta C_{pL} = \frac{\Delta S_d - R\ln\frac{\xi_e}{1-\xi_e}}{\left(\frac{RT}{\xi_e(1-\xi_e)} - 2w\right)}(\Delta H_d + w(1-2\xi_e)) \tag{73}$$

This equation is identical to eq. (17) of Moynihan [61] for $p = p^\circ$.

An alternative and useful expression of the configurational heat capacity, in which ΔS_d does not appear, can be established by substituting (51) in (71). After some calculations, it reads:

$$\Delta C_{pL} = \xi_e\left(\frac{\partial \Delta H_d}{\partial T}\right)_p - T\left(\frac{\partial^2 w}{\partial T^2}\right)_p \xi_e(1-\xi_e) + \frac{\left(\Delta H_d + w(1-2\xi_e) - T\left(\frac{\partial w}{\partial T}\right)_p (1-2\xi_e)\right)^2}{\left(1 - \frac{2w}{RT}\xi_e(1-\xi_e)\right)}\frac{\xi_e(1-\xi_e)}{RT^2} \tag{74}$$

If w is independent of temperature, eq. (74) simplifies to:

$$\Delta C_{pL} = \xi_e \left(\frac{\partial \Delta H_d}{\partial T}\right)_p + \frac{\left(\Delta H_d + w(1-2\xi_e)\right)^2}{\left(1 - \frac{2w}{RT}\xi_e(1-\xi_e)\right)} \frac{\xi_e(1-\xi_e)}{RT^2} \tag{75}$$

If ΔH_d is also independent of temperature, eq. (75) further simplifies to:

$$\Delta C_{pL} = \frac{\left(\Delta H_d + w(1-2\xi_e)\right)^2}{\left(1 - \frac{2w}{RT}\xi_e(1-\xi_e)\right)} \frac{\xi_e(1-\xi_e)}{RT^2} \tag{76}$$

In this form, it is easier to see that when $w = 0$, eq. (24) of the ideal 2-state model is again found. Furthermore, the heat capacity diverges when approaching a spinodal instability because the term in parentheses in the denominator of eq. (76) becomes zero when T is given by eq. (58).

The interaction parameter allows the shape of the evolution of the configurational part of the thermodynamic functions to change radically with temperature, as illustrated in Figure 8.

More precisely, a strongly positive value of the interaction parameter (red curves in Figure 8) results in a sharp peak in heat capacity (Figure 8c), the counterpart of which is an abrupt decrease of the entropy when the liquid cools down (Figure 8b).

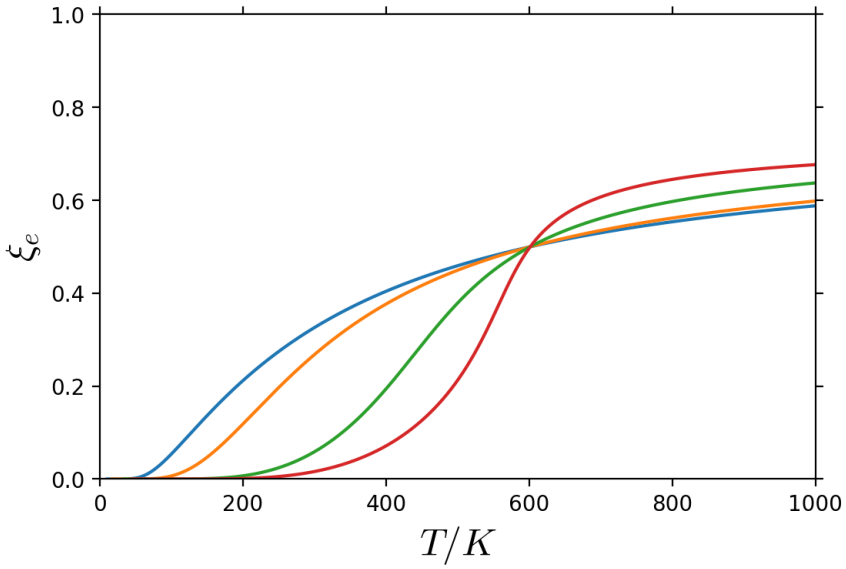

a)

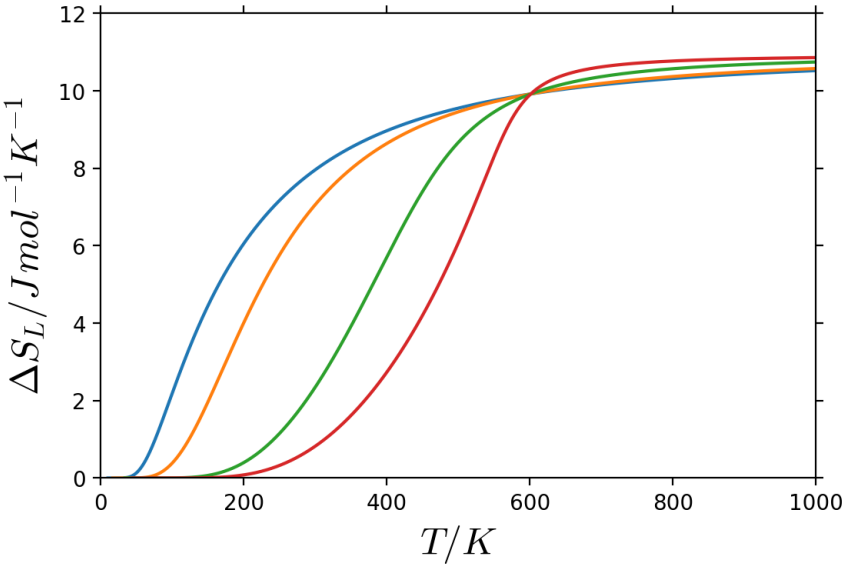

b)

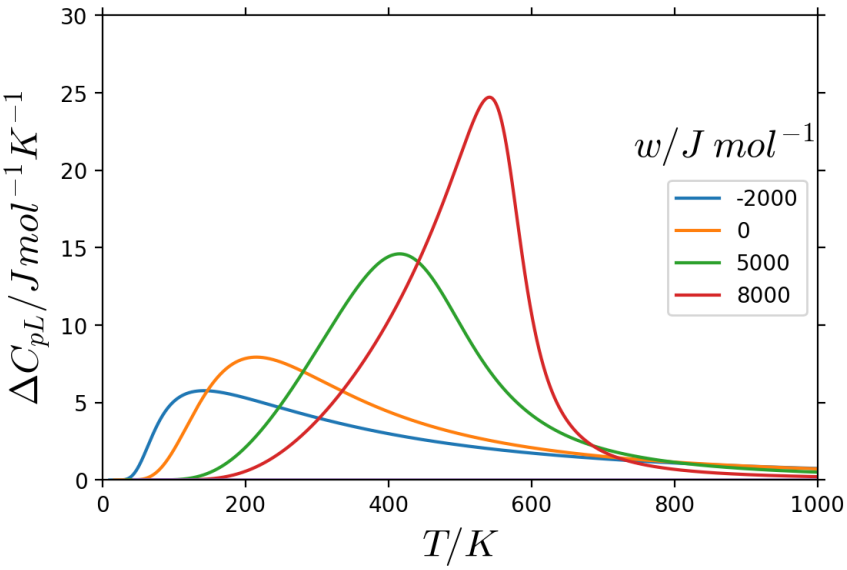

c)

Figure 8. Evolution of a) the fraction of excited units, b) the configurational entropy and c) the configurational heat capacity of the liquid for $\Delta H_d = 5000\ J\ mol^{-1}$, $\Delta S_d = R$ *and various values of* w *given as legend in c).*

6 The regular 2-state model at high pressures

Under ambient pressure, the formalism presented in sections 4 and 5 is sufficient. However, when high pressures are applied to liquids in which the structural entities A and B have different molar volumes, it becomes mandatory to explicitly introduce the mechanical work term in the two-state model.

Following Rapoport [56], Johari [38] or Ponyatovsky [60], we now expand the Gibbs energy difference between the 2 states under the form:

$$\Delta G_d = \Delta E_d + p\Delta V_d - T\Delta S_d \tag{77}$$

By deriving the expression (45) for Gibbs energy with respect to pressure, and using the internal equilibrium condition (47), we show that:

$$V_L = \left(\frac{\partial G_L}{\partial p}\right)_T = V_A^\circ + \xi_e \Delta V_d + \left(\frac{\partial w}{\partial p}\right)_T \xi_e(1-\xi_e) \tag{78}$$

In which, we have noted:

$$\Delta V_d = V_B^\circ - V_A^\circ = \left(\frac{\partial \Delta G_d}{\partial p}\right)_T \tag{79}$$

Which can be positive for "normal" liquids or negative for "abnormal" tetrahedral networks liquids such as H_2O [58]. Equation (78) is identical to equation (9) of [56] noting that Rapoport had taken the opposite sign convention in his notation of the volume difference between the two states.

If the interaction coefficient is independent of the pressure, we find the volume of the ideal solution which is also that of a simple mechanical mixture:

$$V_L = V_A^\circ + \xi_e \Delta V_d \tag{80}$$

This is equation (5.37) on page 146 of [74], equation (11) of [56] which can also been found in [75] (page 3, top of column 2) or eq. (5) of [76].

By denoting the configurational volume $\Delta V_L = V_L - V_A^\circ$ eq. (80) can be rewritten in the condensed form:

$$\Delta V_L = \xi_e \Delta V_d \tag{81}$$

By deriving equation (78) with respect to temperature and rearranging terms, the configurational coefficient of thermal expansion $\Delta\alpha_L$ reads:

$$V_L \Delta\alpha_L = \left(\frac{\partial^2 \Delta G_L}{\partial T \partial p}\right)_{p,T} = \left(\frac{\partial \Delta V_L}{\partial T}\right)_p = \xi_e \left(\frac{\partial \Delta V_d}{\partial T}\right)_p + \left(\frac{\partial^2 w}{\partial T \partial p}\right)_{p,T} \xi_e(1-\xi_e) + \frac{\left(\Delta V_d + \left(\frac{\partial w}{\partial p}\right)_T (1-2\xi_e)\right)\left(\Delta S_d - Rln\frac{\xi_e}{1-\xi_e} - \left(\frac{\partial w}{\partial T}\right)_p (1-2\xi_e)\right)}{\frac{RT}{\xi_e(1-\xi_e)} - 2w} \tag{82}$$

If ΔV_d does not depend on T and w does not depend on T and p, equation (82) simplifies to:

$$V_L \Delta\alpha_L = \frac{\Delta V_d \left(\Delta S_d - Rln\frac{\xi_e}{1-\xi_e}\right)}{\frac{RT}{\xi_e(1-\xi_e)} - 2w} \tag{83}$$

We find equation (18) of Moynihan [61].

The configurational coefficient of compressibility $\Delta\kappa_L$ can be evaluated by deriving eq. (81) with respect to pressure.

It is first needed to evaluate the pressure derivative of the internal equilibrium condition (50). We obtain:

$$\left(\frac{\partial \xi_e}{\partial p}\right)_T = -\frac{\Delta V_d + \left(\frac{\partial w}{\partial p}\right)_T (1-2\xi_e)}{\frac{RT}{\xi_e(1-\xi_e)} - 2w} \tag{84}$$

The rate of change of the structural order parameter with the pressure for the ideal 2-state model is obtained by taking $w = 0$ in eq. (84) yielding:

$$\left(\frac{\partial \xi_e}{\partial p}\right)_T = -\frac{\Delta V_d}{RT}\xi_e(1-\xi_e) \tag{85}$$

This equation has already been obtained, notably by Kauzmann (see eq. (12) of [77].

The configurational coefficient of compressibility $\Delta\kappa_L$ reads:

$$V_L \Delta\kappa_L = -\left(\frac{\partial^2 \Delta G_L}{\partial p^2}\right)_T = -\left(\frac{\partial \Delta V_L}{\partial p}\right)_T = -\xi_e \left(\frac{\partial \Delta V_d}{\partial p}\right)_T - \left(\frac{\partial^2 w}{\partial p^2}\right)_{p,T} \xi_e(1-\xi_e) + \frac{\left(\Delta V_d + \left(\frac{\partial w}{\partial p}\right)_T (1-2\xi_e)\right)^2}{\frac{RT}{\xi_e(1-\xi_e)} - 2w} \tag{86}$$

If ΔV_d and w do not depend on p, eq. (86) simplifies to:

$$V_L \Delta\kappa_L = \frac{\Delta V_d^2}{\frac{RT}{\xi_e(1-\xi_e)} - 2w} \tag{87}$$

We find equation (19) of Moynihan [61][2].

The phase diagram of the model can be calculated.

The $p(T)$ expression is simply obtained from the condition of coexistence *(55)* under the form:

$$p = \frac{T\Delta S_d - \Delta E_d}{\Delta V_d} \tag{88}$$

Particularly, at the critical point (T_c, p_c):

$$p_c = \frac{T_c\Delta S_d - \Delta E_d}{\Delta V_d} \tag{89}$$

We define the dimensionless pressure p^* according to:

$$p^* = \frac{p}{p_c} \tag{90}$$

By substituting ΔV_d in (88) using (89), a dimensionless form of the condition of coexistence is obtained:

$$p^* = \frac{T^*\frac{\Delta S_d}{R} - \frac{\Delta E_d}{RT_c}}{\frac{\Delta S_d}{R} - \frac{\Delta E_d}{RT_c}} \tag{91}$$

Injecting (77) in the internal equilibrium condition (50) and using (53) and (89) yields a new dimensionless form of the internal equilibrium condition:

$$p^* = \frac{T^*\left(\frac{\Delta S_d}{R} - \ln\frac{\xi_e}{1-\xi_e}\right) - \frac{\Delta E_d}{RT_c} - 2(1-2\xi_e)}{\frac{\Delta S_d}{R} - \frac{\Delta E_d}{RT_c}} \tag{92}$$

The two spinodal curves can be obtained as follows. For given $T^* < 1$, the two corresponding values of the internal variable ξ_{inf} and ξ_{sup} are calculated using (64), then the two corresponding pressure values p^*_{inf} and p^*_{sup} are calculated with (92) using (T^*, ξ_{inf}) and (T^*, ξ_{sup}) as inputs.

The pressure-temperature phase diagram of the regular 2-state model is plotted in dimensionless coordinates in Figure 9 using equations (91) and (92).

[2] Note that expressions of the configurational heat capacity (76), thermal expansion (83) and compressibility (87) coefficients have also been established by Ponyatovsky [60] however his equations (11) and (12) are misprinted. The right hand side of his eq. (11) in fact corresponds to the left hand side of his eq. (12) while the right hand side of his eq. (12) corresponds to the left hand side of eq. (11).

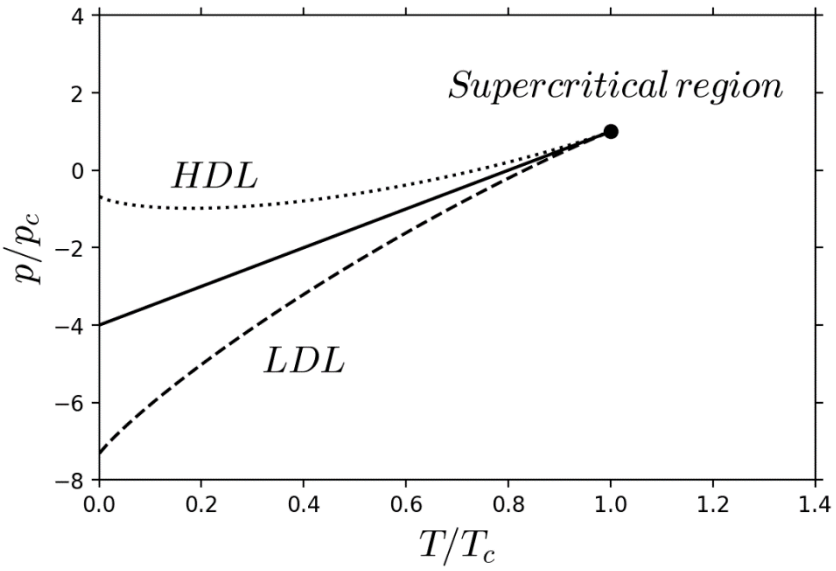

Figure 9. Pressure-temperature phase diagram of the regular 2-state model in dimensionless coordinates. The diagram is plotted with the dimensionless parameter values $\Delta S_d/R = 3$ *and* $\Delta E_d/\ RT_c\ = 2.4$ *taken as a typical example eq. (10) from* [61]. *Solid line is the coexistence curve between a High Density Liquid (HDL) and a Low Density Liquid (LDL) terminating at the critical point (black dot). The dashed and dotted curves are the HDL and LDL spinodals respectively.*

By taking the derivative of the internal equilibrium condition *(50)* with respect to pressure at constant ξ_e, and considering parameters $\Delta E_d, \Delta V_d, \Delta S_d$ as constants, we obtain:

$$\left(\frac{dT}{dp}\right)_{\xi_e} = \frac{\Delta V_d}{\Delta S_d - R\ ln\frac{\xi_e}{1-\xi_e}} \tag{93}$$

Hence, with constant parameters, an isofraction curve is a straight line whose slope is given by eq. (93) and the intercept can be calculated using the internal equilibrium condition (51).

Considering the parameters $\Delta E_d, \Delta S_d, \Delta V_d$ as constants, the Clapeyron slope of the coexistence line is:

$$\frac{dp}{dT} = \frac{\Delta S_d}{\Delta V_d} \tag{94}$$

7 Two examples

Disregarding the modeling of the background contribution, application of the regular formalism to a real substance requires to adjust the values of the 4 parameters $\Delta E_d, \Delta V_d, \Delta S_d$ and w of the model. In this section, two examples are selected from literature to highlight various types of relevant calculations that can be performed with the model.

Rapoport [57] applied the model to explain the melting curve maxima observed at high pressures for certain elements such as Cs or Te. For Te, Rapoport assumed that the liquid was a mixture of Te(I) and Te(III) species corresponding, in terms of short range order, to their crystalline counterparts the Te(I) low-pressure crystal being a p-type semi-conductor and the Te(III) high-pressure crystal being metallic. In this case, the excited level of the model corresponds to the Te(III) metallic species. He tuned the parameters of the model using a complex optimization procedure based mainly on Hall coefficient and electrical conductivity data in the liquid, assuming a negligible contribution of Te(I) species to these physical quantities. The optimized values of the parameters are listed in Table 2.

Table 2. Parameters of the regular 2-state model from 2 literature studies. R is the gas constant.

Reference	Substance	ΔE_d	ΔV_d	ΔS_d	w
		$/J\ mol^{-1}$	$/m^3\ mol^{-1}$	$/J\ mol^{-1}K^{-1}$	$/J\ mol^{-1}$
[57]	Te	41×4.184	$-1.5\ 10^{-6}$	-0.154×4.184	$2.01R \times 737.15$
[61]	H_2O	1940	$-4.5\ 10^{-6}$	$0.98R$	3610

We have recalculated figure 3 of the original article in the Figure 10 below. The isofraction lines calculated using equations (93) and (51) show that the Te(III) species predominates in the liquid at high pressures. The experimental data on the melting line of Te(I) crystal of Stishov & Tikhomirova [78] and Klement et al. [79] are superimposed on the figure. In our plotting procedure, a cubic fit of the data of Stishov & Tikhomirova [78] is used as a lower bound of the calculated liquid isofraction lines.

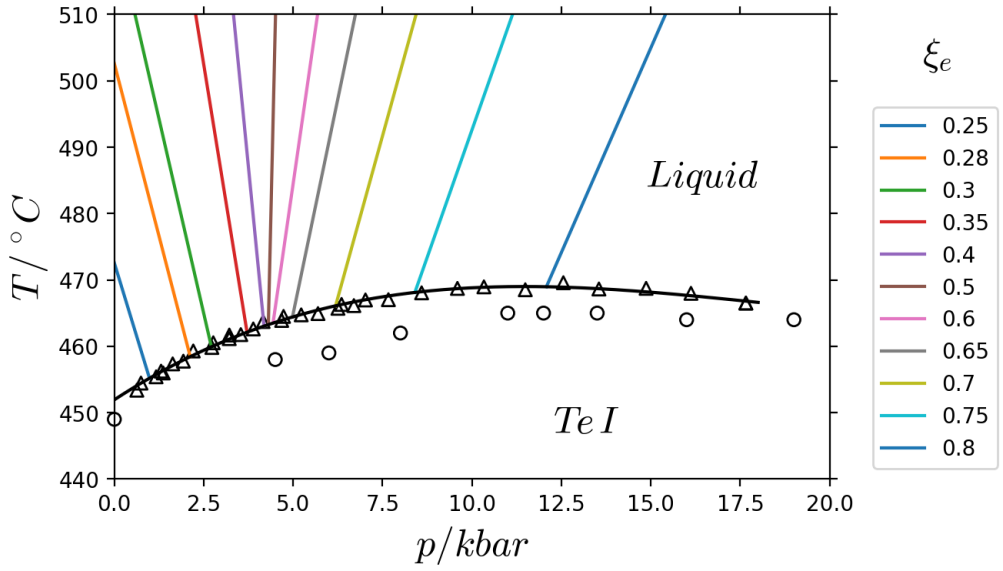

Figure 10. $T-p$ phase diagram of pure tellurium. Scatter symbols are experimental points of Stishov & Tikhomirova (△) [78] and Klement et al. (○) [79]. The fan-shaped cluster of colored curves are the isofraction lines in the liquid calculated with the regular 2-state model and parameter values from Rapoport [57]. The solid black line is a cubic fit to the datapoints of Stishov & Tikhomirova and materializes the limit to the extension of the liquid isofraction lines.

The study of Rapoport concentrates on the low pressure range, up to 20 kbar, of the $T-p$ phase diagram of pure Tellurium. More recently, Brazkhin et al. [80] have discovered a liquid-liquid equilibrium line in the liquid domain at higher pressure and temperature. Modelling this phase separation would be possible using the regular 2-state model but would require a different parametrization of the model than Rapoport.

The case of water, one of the most studied liquid, is selected as the second example. A recent review of LL phase separation and polyamorphism phenomena in supercooled water has been carried out by Tanaka [52]. The existence of LL phase separation remains controversial because of the difficulty of observing it directly. It is likely to be hidden in the supercooled regime at temperatures below the homogeneous nucleation temperature of crystalline ice. However, the evolutions of the susceptibility coefficients, i.e. heat capacity, thermal expansivity and isothermal compressibility, as a function of temperature show striking anomalies. Many authors have attempted to model these thermodynamic anomalies using two-state descriptions. An extensive list of early works can be found in the critical analysis of Kauzmann [77], more recent works were already listed in section 3. Different types of 2-state models have in fact been used: ideal, regular/cooperative, entropy-driven athermal and mixed models combining the latter two.

The most comprehensive descriptions of water using two-state models, based on extensive experimental datasets over wide temperature and pressure ranges, come from the work of Anisimov and his colleagues [65] [66] [67] [81] [82]. However, in these sophisticated models, the analytical expressions used to formulate i) the Gibbs energy difference between the 2 states and ii) the background contributions to the thermodynamic quantities are quite different from those commonly used in 3rd generation CALPHAD models. Moreover, around 20 parameter values need to be adjusted in these descriptions.

Therefore, for the application to water, we have instead chosen the much simpler model, and parameter values (Table 2), of Moynihan [61] because it is consistent with the formalism presented in sections 4 to 6. This formalism only represents the configurational part of the thermodynamic functions and does not include the background contributions varying slowly with temperature and pressure. In order to be able to compare the model results with the available experimental data, in the present work, rough estimates of the background contributions were made as constant values where necessary.

An estimation of the density of water in the stable and metastable temperature range under atmospheric pressure is also required for comparing the calculated thermal expansion and compressibility with experimental data. The density of water was estimated by combining the experimental dataset of Hare & Sorensen [83] in the supercooled range with the data from the Handbook of Chemistry & Physics [84] between 0 and 100°C. The obtained dataset of 495 points was then simply fitted by a 6th degree polynomial.

The heat capacity, the coefficient of thermal expansion and the isothermal compressibility calculated at atmospheric pressure with the regular 2-state model are plotted against temperature and compared with experimental results from various literature studies in Figure 11. A global good agreement is observed which could probably be improved with a more thorough assessment of the background contributions.

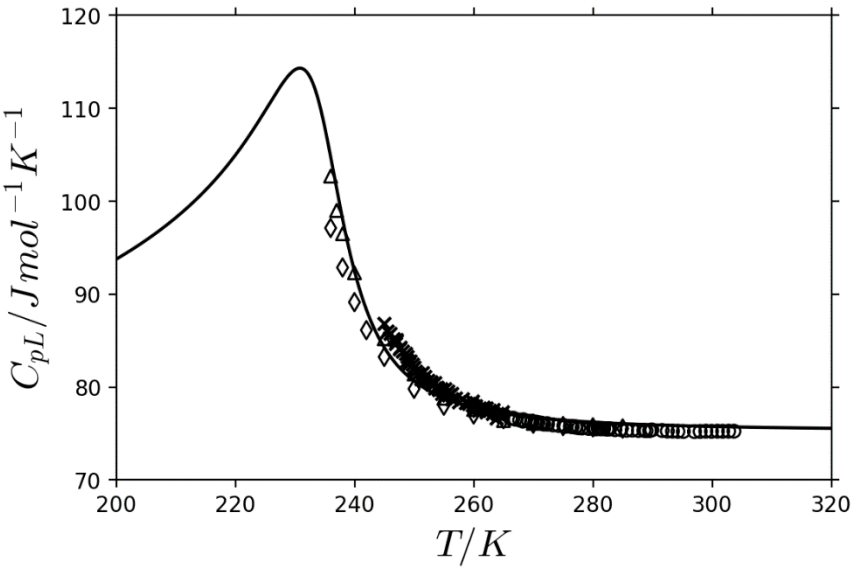

a) Scatter symbols are experimental points of Anisimov et al. (○) [85]*, Angell et al.* (△) [86]*, Tombari et al.* (×) [87] *and Archer & Carter* (◊) [88]. *Solid line is calculated with eq.* (76) *adding a constant* $C_{p0} = 75.25\ J\ mol^{-1}\ K^{-1}$ *background contribution.*

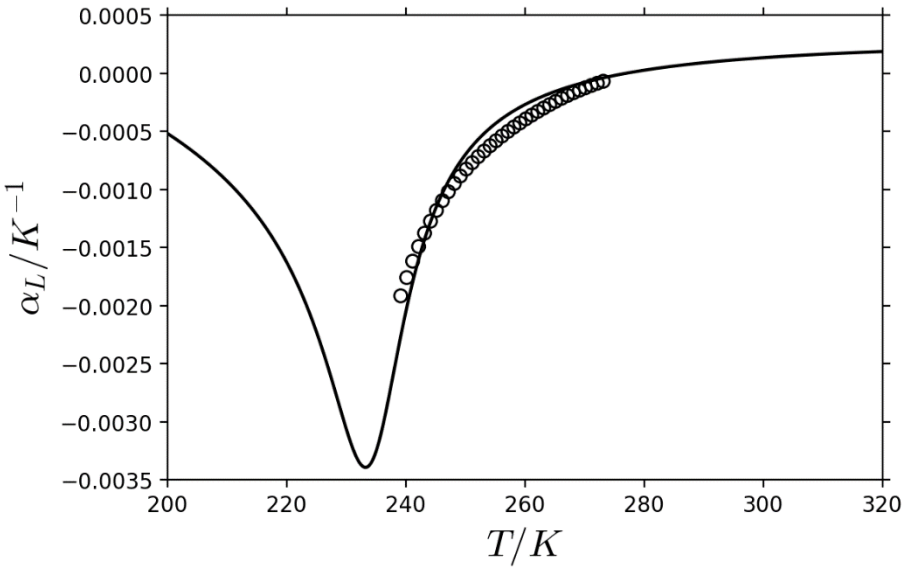

b) Scatter symbols (○) are experimental points of Hare &Sorensen [83], *solid line is calculated with eq.* (83) *and adding a constant* $\alpha_{L0} = 3\ 10^{-4}\ K^{-1}$ *background contribution.*

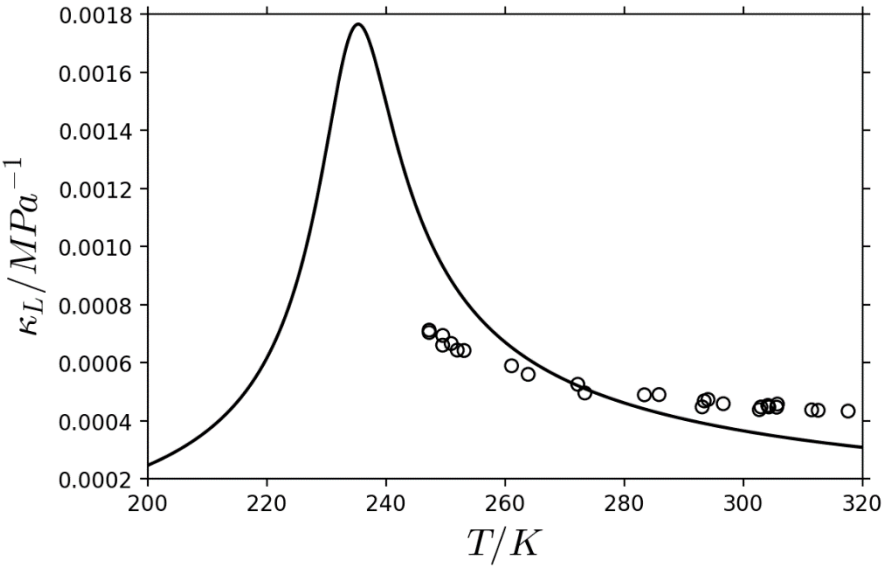

c) Scatter symbols (○) are experimental points of Speedy &Angell [89], *solid line is calculated with eq.* (87) *and adding a constant* $\kappa_{L0} = 8\ 10^{-5} MPa^{-1}$ *background contribution.*

Figure 11. Evolution of the a) heat capacity b) thermal expansion coefficient and c) isothermal compressibility of water with temperature at atmospheric pressure. Solid lines are calculated with the regular 2-state model and parameters from Moynihan [61]. *Where required, the molar volume of water is estimated using the procedure described in the text.*

In Mishima's experiment [90], amorphous ice is submitted to a compression-decompression-recompression cycle at an average temperature of 135 ± 5 K, very close to the value of the glass transition temperature (136 K) traditionally accepted for water [91] [92]. This T_g value remains however controversial as it has been estimated at $165 \pm 5\ K$ by Angell and coworkers [93] [94] [95]. Mishima discovered a reversible first order transition between a Low Density Amorphous (LDA) phase and a High Density Amorphous (HDA) phase. Moynihan used Mishima's data to optimize the model parameter values, so we have tried to reproduce Mishima's experimental results with the parameter set in Table 2.

The volume calculated with eq. (80) is compared to the experimental data in Figure 12. In performing this comparison, it is further assumed in the present work that, in eq. (80), the volume of the A entities depends on pressure according to:

$$V_A^\circ = V_0 \exp\left(-\kappa_{L0}(p - p_0)\right) \tag{95}$$

Where p_0 is the atmospheric pressure and V_0 is the volume of amorphous ice under atmospheric pressure at 135 K estimated to be $V_0 \approx 1.09\, cm^3\, g^{-1}$ from Mishima's data. The same constant background compressibility value $\kappa_{L0} = 8\, 10^{-5} MPa^{-1}$ is used to calculate Figure 11c and Figure 12. A good agreement is observed between the calculated curve and the experimental points in Figure 12.

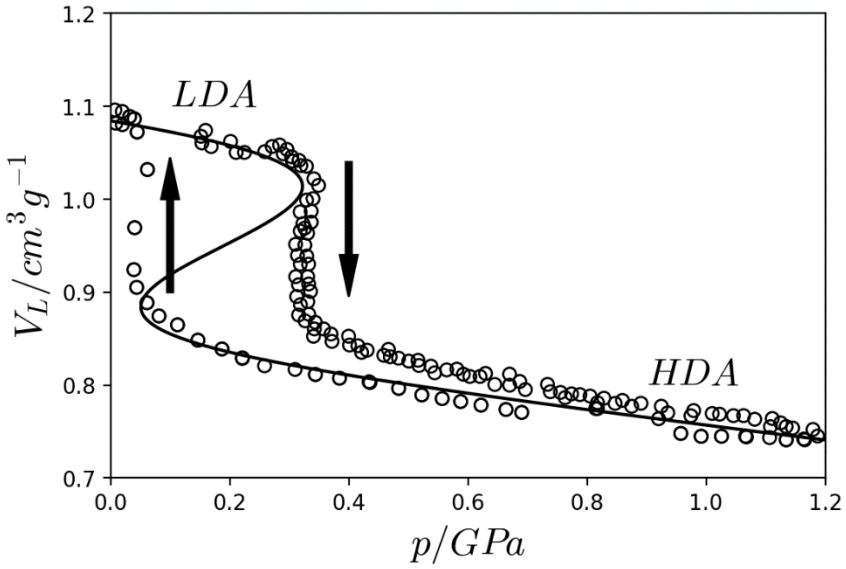

Figure 12. Evolution of the volume of amorphous ice during a compression-decompression-recompression cycle at $T = 135 \pm 5\, K$. *Scatter symbols* (○) *are experimental points of Mishima* [90]. *The solid line is calculated with eq. (80) using parameters from Moynihan* [61]. T*he effect of the pressure on the background contribution is estimated using the procedure described in the text. The downward and upward black arrows indicate the branches of the experimental curve followed on compression and decompression respectively. The overall shape is typical of a 1st order transition occurring abruptly on reaching spinodal instabilities at* $p \approx 0.32\, GPa$ *on compression and* $p \approx 0.05\, GPa$ *on decompression. The portion of the calculated curve for which* $(\partial V_L/\partial p)_T > 0$ *corresponds to mechanically unstable states.*

The metastable temperature-pressure phase diagram of liquid/glassy water is plotted in Figure 13. At $T = 135 \pm 5\, K$ the experimentally observed LDA → HDA transition on compression and HDA → LDA transition on decompression both coincide with the calculated spinodal curves as already shown in Figure 12. In Figure 13, it can also be seen that the so-called Widom line (dotted line) rather than the LL line (solid line) is crossed when cooling liquid water under atmospheric pressure. Thus, there is no discontinuity in the response coefficients plotted against temperature in Figure 11 a) to c), but peaks are observed.

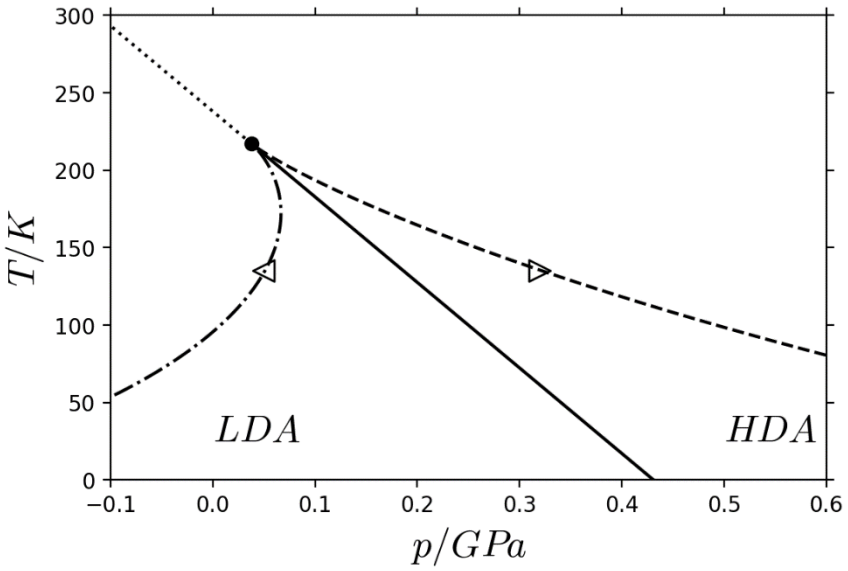

Figure 13. $T - p$ *phase diagram of liquid/amorphous water according to the regular 2-state model of Moynihan* [61]. *Solid line is the LDA-HDA coexistence curve terminating at the critical point* (•). *The extension of the coexistence curve beyond the critical point is the so-called Widom line (dotted line). The dashed and dash-dotted curves are the two spinodals. In Mishima's experiment* [90] *at* $T = 135 \pm 5\ K$, *the LDA* → *HDA transition is observed around* $p \approx 0.32\ GPa$ *on compression* (▷) *and the HDA* → *LDA transition occurs around* $p \approx 0.05\ GPa$ *on decompression* (◁).

8 Discussion

We now return to the main focus of the present article which is the interest of the regular 2-state model for CALPHAD type modeling.

Let us first consider the 3rd generation descriptions of the pure elements already available and involving only the temperature variable. For the subset of elements (Al, Au, Fe, Ga, In, Mn, Pb, Sn) listed in Table 1 for which experimental heat capacity data are available for the liquid phase, only Pb shows a fairly strong increase in heat capacity as the temperature is decreased below the melting point. The experimentally observed increase in heat capacity appears to be slightly steeper (see fig. 8b of [15]) than that calculated with the ideal 2-state model. In this case, it is possible that the agreement could be improved by using the regular 2-state model, but this has not been attempted in the present work.

To our knowledge, Sn is the only element for which a complete $T - p$ 3rd generation description [17] is available. In this literature study, the liquid phase is described using the ideal 2-state model neglecting the possible effect of the pressure variable on the Gibbs energy difference between the 2 states. It is suggested in the present work that such a modification might be relevant in cases where a significant difference in volume between the two states is expected.

The regular formalism presented in this article is most likely to bring significant improvements and find its most useful applications in the following cases.

Firstly, on substances for which extensive experimental data are available concerning the liquid phase, both at the stable and metastable, supercooled, states and the glassy phase. The thermodynamic behavior of strong and fragile liquids is strikingly different. This difference in behavior is well illustrated by Figure 4 in [25], despite its qualitative nature. By comparison with the quantitative Figure 8 in the present paper, it can be concluded that, as already pointed out by Angell & Moynihan [37], increasing the value of the parameter w increases the fragility of the liquid. Hence, the blue (slightly attractive A-B interaction) or orange (ideal A-B solution) curves correspond to strong liquid behavior while the red curves (repulsive A-B interaction) describe the behavior of a fragile liquid. Hence, the regular 2-state model offers the possibility to simulate the main archetypes of glass forming liquids and can offer more flexibility in the fitting process, even in the case of strong liquids such as GeO_2 and SiO_2.

Secondly, in $T-p$ unary phase diagrams, the occurrence of a melting maximum for a specific crystalline phase at high pressure can be explained using a regular 2-state model [50] [56]. The case of Te was considered in former section. Another example is provided by the phase diagram of pure C, in which the graphite [96], diamond and BC8 [97] phases all show this characteristic. Occurrence of a melting maximum is probably not a so rare event when the $T-p$ plane is explored.

Thirdly, unlike its ideal counterpart, the regular 2-state model is also able to simulate LL transitions in pure substances. In the case of water discussed above, the transition occurs in a $T-p$ region of the phase diagram where the liquid is metastable compared to crystalline ice. Such LL transitions are very difficult to observe experimentally because they can be easily masked by crystallization or by the occurrence of the kinetic glass transition on cooling. However, for other pure substances such as Bismuth [98], a LL transition has been detected in the domain of liquid stability. Moreover, in the case of Sulphur, and for the first time, the critical point terminating the LL coexistence curve at high pressure and temperature could be determined [99]. It is also worth adding that an accurate knowledge of the critical point is of great value for tuning the parameters of the regular 2-state model using equations (52), (53), (54) and (89). LL transitions are in fact suspected to occur in many substances including pure elements such as Bi, C, Ge, P, S, Si, pure oxides such as GeO_2 and SiO_2, and organic substances like TriPhenyl Phosphite (TPP) [100]. Unambiguous demonstration of their existence is generally missing owing to the high experimental difficulties involved. The reader is referred to the comprehensive reviews of Wilding et al. [51] and Tanaka [52] for a more thorough analysis of these issues and more exhaustive list of chemical systems where possible existences of LL transitions are under investigation.

We would like to add some general considerations to end this discussion. It is not excluded, and even strongly suggested by some authors, that more than two liquid polymorphs may exist, especially in cases where several crystalline phases are successively stabilized by the pressure increase. Indeed, phase diagrams in which the liquid phase has several LL coexistence lines and corresponding critical points have been drawn schematically notably by Tanaka (fig. 2 of [63]) or McMillan (fig. 1c of [50]).

In most CALPHAD modelling work, the gas and liquid phases are treated as separate phases. However, the most obvious polymorph of any liquid is the gas phase itself, as it is common knowledge that the thermodynamic description of the liquid and gas phases can be unified through the van der Waals fluid EOS. Interestingly, Anisimov et al. [101] have proposed a general thermodynamic formalism to describe fluid polyamorphism. The approach elegantly combines a regular 2-state model with a van der Waals model, or alternatively a lattice-gas model. To be more precise, the background contribution of the 2-state model (the A ground-state) is modelled as a van der Waals fluid or a lattice-gas, two descriptions that are qualitatively close [102]. The approach of Anisimov et al. is therefore able to describe the liquid-liquid and liquid-vapor equilibria in a pure substance in a unified way.

In relation to the gas, one may wonder about the nature of the liquid occupying the other end of the entropy scale, i.e. a liquid polymorph having a small excess entropy over the crystal, which can be possibly formed through a 1st order LL transition. Such a liquid could be considered as an "ideal glass".

Conclusion

The ideal 2-state model is exclusively used for describing the liquid phase in 3rd generation CALPHAD work. The present article does not invalidate this earlier work, but rather suggests that the regular 2-state model may represent a valuable complementary modeling tool that considerably broadens the spectrum of phenomena that can be described. The application of the regular 2-state model to a new test case will be the subject of a future work. This model should only be used if it significantly improves the description compared to the ideal model, and its applicability in a multicomponent system should also be verified.

Methodology

The numerical calculations required in this work were performed using a home-made Python program and the Numpy package, instead of a more conventional CALPHAD software. For this reason, there is no TDB file for this work. All figures are generated with the Matplotlib library.

Acknowledgments

Jacques Rogez (IM2NP, Marseille) for useful comments on the manuscript.

Abbreviations

EOS Equation Of State

FTS Fragile To Strong (transition)

LDA Low Density Amorphous (phase)

LDL Low Density Liquid

LL Liquid-Liquid (transition or phase separation or coexistence)

HDA High Density Amorphous (phase)

HDL High Density Liquid

References

[1] J. Ågren, Thermodynamics of Supercooled Liquids and their Glass Transition, Phys. Chem. Liq. 18 (1988) 123–139. https://doi.org/10.1080/00319100701344644.

[2] J. Agren, B. Cheynet, M.T. Clavaguera-mora, K. Hack, J. Hertz, F. Sommer, U. Kattner, Workshop on thermodynamic models and data for pure elements and other endmembers of solutions, Calphad. 19 (1995) 449–480. https://doi.org/10.1016/0364-5916(96)00003-X.

[3] C. a. Becker, J. Ågren, M. Baricco, Q. Chen, S. a. Decterov, U.R. Kattner, J.H. Perepezko, G.R. Pottlacher, M. Selleby, Thermodynamic modelling of liquids: CALPHAD approaches and contributions from statistical physics, Phys. Status Solidi. 52 (2014) 33–52. https://doi.org/10.1002/pssb.201350149.

[4] A. Dinsdale, O. Zobac, A. Kroupa, A. Khvan, Use of third generation data for the elements to model the thermodynamics of binary alloy systems: Part 1 – The critical assessment of data for the Al-Zn system, Calphad Comput. Coupling Phase Diagrams Thermochem. 68 (2020) 101723. https://doi.org/10.1016/j.calphad.2019.101723.

[5] Z. He, B. Kaplan, H. Mao, M. Selleby, The third generation Calphad description of Al–C including revisions of pure Al and C, Calphad Comput. Coupling Phase Diagrams Thermochem. 72 (2021) 102250. https://doi.org/10.1016/j.calphad.2021.102250.

[6] A. V. Khvan, I.A. Uspenskaya, N.M. Aristova, Q. Chen, G. Trimarchi, N.M. Konstantinova, A.T. Dinsdale, Description of the thermodynamic properties of pure gold in the solid and liquid states from 0 K, Calphad Comput. Coupling Phase Diagrams Thermochem. 68 (2020) 101724. https://doi.org/10.1016/j.calphad.2019.101724.

[7] O. Tolochko, J. Ågren, Thermodynamic properties of supercooled Fe-B liquids—A theoretical and experimental study, J. Phase Equilibria. 21 (2000) 19–24. https://doi.org/10.1361/105497100770340372.

[8] S. Bigdeli, Q. Chen, M. Selleby, A New Description of Pure C in Developing the Third Generation of Calphad Databases, J. Phase Equilibria Diffus. 39 (2018) 832–840. https://doi.org/10.1007/s11669-018-0679-3.

[9] Z. Li, S. Bigdeli, H. Mao, Q. Chen, M. Selleby, Thermodynamic evaluation of pure Co for the third generation of thermodynamic databases, Phys. Status Solidi Basic Res. 254 (2017). https://doi.org/10.1002/pssb.201600231.

[10] Q. Chen, B. Sundman, Modeling of Thermodynamic Properties for Bcc, Fcc, Liquid, and Amorphous Iron, J. Phase Equilibria. 22 (2001) 631–644. https://doi.org/10.1361/105497101770332442.

[11] Z. He, F. Haglöf, Q. Chen, A. Blomqvist, M. Selleby, A Third Generation Calphad Description of Fe: Revisions of Fcc, Hcp and Liquid, J. Phase Equilibria Diffus. 43 (2022) 287–303. https://doi.org/10.1007/s11669-022-00961-w.

[12] A.V. Khvan, N. Konstantinova, I.A. Uspenskaya, A.T. Dinsdale, A.I. Druzhinina, A. Ivanov, I. Bajenova, A description of the thermodynamic properties of pure indium in the solid and liquid states from 0 K, Calphad. 79 (2022) 102484. https://doi.org/10.1016/j.calphad.2022.102484.

[13] S. Bigdeli, H. Mao, M. Selleby, On the third-generation Calphad databases: An updated description of Mn, Phys. Status Solidi Basic Res. 252 (2015) 2199–2208. https://doi.org/10.1002/pssb.201552203.

[14] E.D. Alvares, W.J. Botta, J. Ågren, A. Costa e Silva, An assessment of Fe-Nb-B melts using the two-state liquid model, Calphad Comput. Coupling Phase Diagrams Thermochem. 68 (2020) 101692. https://doi.org/10.1016/j.calphad.2019.101692.

[15] A.V. Khvan, A.T. Dinsdale, I.A. Uspenskaya, M. Zhilin, T. Babkina, A.M. Phiri, A thermodynamic description of data for pure Pb from 0 K using the expanded Einstein model for the solid and the two state model for the liquid phase, Calphad. 60 (2018) 144–155. https://doi.org/10.1016/j.calphad.2017.12.008.

[16] A. V. Khvan, T. Babkina, A.T. Dinsdale, I.A. Uspenskaya, I. V. Fartushna, A.I. Druzhinina, A.B. Syzdykova, M.P. Belov, I.A. Abrikosov, Thermodynamic properties of tin: Part I Experimental investigation, ab-initio modelling of α-, β-phase and a thermodynamic description for pure metal in solid and liquid state from 0 K, Calphad Comput. Coupling Phase Diagrams Thermochem. 65 (2019) 50–72. https://doi.org/10.1016/j.calphad.2019.02.003.

[17] G. Deffrennes, P. Faure, F. Bottin, J.M. Joubert, B. Oudot, Tin (Sn) at high pressure: Review, X-ray diffraction, DFT calculations, and Gibbs energy modeling, J. Alloys Compd. 919 (2022) 165675. https://doi.org/10.1016/j.jallcom.2022.165675.

[18] Z. He, M. Selleby, A third generation Calphad description of pure W, Mater. Chem. Phys. 276 (2022) 125445. https://doi.org/10.1016/j.matchemphys.2021.125445.

[19] A. V. Khvan, A.T. Dinsdale, Q. Chen, Use of third generation data for the elements to model the thermodynamics of binary alloy systems: Part 2 – The critical assessment of data for the Pb-Sn system, Calphad Comput. Coupling Phase Diagrams Thermochem. 76 (2022) 1–10. https://doi.org/10.1016/j.calphad.2022.102396.

[20] Z. He, M. Selleby, A third generation Calphad description of W–C including a revision of liquid C, Calphad. 78 (2022) 102449. https://doi.org/10.1016/j.calphad.2022.102449.

[21] P. Benigni, CALPHAD modeling of the glass transition for a pure substance, coupling thermodynamics and relaxation kinetics, Calphad. 72 (2021) 102238. https://doi.org/10.1016/j.calphad.2020.102238.

[22] G. Deffrennes, N. Jakse, C.M.S. Alvares, I. Nuta, A. Pasturel, A. Khvan, A. Pisch, Thermodynamic modelling of the Ca–O system including 3rd generation description of CaO and CaO2, Calphad Comput. Coupling Phase Diagrams Thermochem. 69 (2020). https://doi.org/10.1016/j.calphad.2020.101764.

[23] I. Bajenova, A. Khvan, A. Dinsdale, A. Kondratiev, Implementation of the extended Einstein and two-state liquid models for thermodynamic description of pure SiO2 at 1 atm, Calphad Comput.

Coupling Phase Diagrams Thermochem. 68 (2020) 101716. https://doi.org/10.1016/j.calphad.2019.101716.

[24] I. Bajenova, A. Khvan, M. Derevyanko, N. Aristova, A. Dinsdale, A. Kondratiev, A. Pisch, Third-generation CALPHAD description of pure GeO2 at 1 atm, Calphad Comput. Coupling Phase Diagrams Thermochem. 74 (2021) 102299. https://doi.org/10.1016/j.calphad.2021.102299.

[25] C.A. Angell, Perspectives on the Glass Transition, J. Phys. Chem. Solids. 49 (1988) 863–871. https://doi.org/10.1016/0022-3697(88)90002-9.

[26] C.A. Angell, Entropy and fragility in supercooling liquids, J. Res. Natl. Inst. Stand. Technol. 102 (1997) 171. https://doi.org/10.6028/jres.102.013.

[27] R. Böhmer, K.L. Ngai, C.A. Angell, D.J. Plazek, Nonexponential relaxations in strong and fragile glass formers, J. Chem. Phys. 99 (1993) 4201–4209. https://doi.org/10.1063/1.466117.

[28] G. Adam, J.H. Gibbs, On the Temperature Dependence of Cooperative Relaxation Properties in Glass-Forming Liquids, J. Chem. Phys. 43 (1965) 139–146. https://doi.org/10.1063/1.1696442.

[29] L.M. Martinez, C.A. Angell, A thermodynamic connection to the fragility of glass-forming liquids, Nature. 410 (2001) 663–667. https://doi.org/10.1038/35070517.

[30] R.J. Speedy, Relations between a Liquid and Its Glasses, J. Phys. Chem. B. 103 (1999) 4060–4065. https://doi.org/10.1021/jp983830w.

[31] G.P. Johari, A resolution for the enigma of a liquid's configurational entropy-molecular kinetics relation, J. Chem. Phys. 112 (2000) 8958–8969. https://doi.org/10.1063/1.481509.

[32] S. Sastry, The relationship between fragility, configurational entropy and the potential energy landscape of glass-forming liquids, Nature. 409 (2001) 164–167. https://doi.org/10.1038/35051524.

[33] G.P. Johari, Contributions to the entropy of a glass and liquid, and the dielectric relaxation time, J. Chem. Phys. 112 (2000) 7518–7523. https://doi.org/10.1063/1.481349.

[34] C.A. Angell, Formation of Glasses from Liquids and Biopolymers, Science (80-.). 267 (1995) 1924–1935. https://doi.org/10.1126/science.267.5206.1924.

[35] J.A. Golczewski, H.J. Seifert, F. Aldinger, A Thermodynamic Model of Amorphous Silicates, Calphad. 22 (1998) 381–396.

[36] C.A. Angell, B.E. Richards, V. Velikov, Simple glass-forming liquids: their definition, fragilities, and landscape excitation profiles, J. Phys. Condens. Matter. 11 (1999) A75–A94. https://doi.org/10.1088/0953-8984/11/10A/005.

[37] C. Austen Angell, C.T. Moynihan, Ideal and cooperative bond-lattice representations of excitations in glass-forming liquids: excitation profiles, fragilities, and phase transitions, Metall. Mater. Trans. B Process Metall. Mater. Process. Sci. 31 (2000) 587–596. https://doi.org/10.1007/s11663-000-0095-y.

[38] G.P. Johari, A Defect Theory for the Glass-Transition and Residual Entropy of Hyperquenched Water, J. Chem. Phys. 98 (1993) 7324–7329. https://doi.org/10.1063/1.464725.

[39] I. Prigogine, R. Defay, Chemical Thermodynamics, Longmans, Greens and Co., 1954.

[40] R.P.H. Gasser, W.G. Richards, An Introduction to Statistical Thermodynamics, World Scientific, 1995. https://doi.org/10.1007/978-3-030-53658-9_1.

[41] A.T. Dinsdale, SGTE data for pure elements, Calphad. 15 (1991) 317–425. https://doi.org/10.1016/0364-5916(91)90030-N.

[42] G. Grimvall, Thermophysical Properties of Materials - Enlarged and revised edition, Elsevier Science B. V., 1999.

[43] S. V. Nemilov, Thermodynamic and Kinetic Aspects of the Vitreous State, CRC Press, 1995.

[44] C.A. Angell, K.J. Rao, Configurational excitations in condensed matter, and the "Bond Lattice" model for the liquid-glass transition, J. Chem. Phys. 57 (1972) 470–481. https://doi.org/10.1063/1.1677987.

[45] M. Goldstein, Glass and other relaxations in liquids, Faraday Symp. Chem. Soc. 6 (1972) 7. https://doi.org/10.1039/fs9720600007.

[46] C.A. Angell, Ten questions on glassformers, and a real space `excitations' model with some answers on fragility and phase transitions, J. Phys. Condens. Matter. 12 (2000) 6463–6475. https://doi.org/10.1088/0953-8984/12/29/318.

[47] P.H. Poole, T. Grande, F. Sciortino, H.E. Stanley, C.A. Angell, Amorphous polymorphism, Comput. Mater. Sci. 4 (1995) 373–382. https://doi.org/10.1016/0927-0256(95)00044-9.

[48] P.H. Poole, T. Grande, C.A. Angell, P.F. McMillan, Polymorphic phase transitions in liquids and glasses, Science (80-.). 275 (1997) 322–323. https://doi.org/10.1126/science.275.5298.322.

[49] V. V. Brazhkin, A.G. Lyapin, High-pressure phase transformations in liquids and amorphous solids, J. Phys. Condens. Matter. 15 (2003) 6059–6084. https://doi.org/10.1088/0953-8984/15/36/301.

[50] P.F. McMillan, Polyamorphic transformations in liquids and glasses, J. Mater. Chem. 14 (2004) 1506. https://doi.org/10.1039/b401308p.

[51] M.C. Wilding, M. Wilson, P.F. McMillan, Structural studies and polymorphism in amorphous solids and liquids at high pressure, Chem. Soc. Rev. 35 (2006) 964. https://doi.org/10.1039/b517775h.

[52] H. Tanaka, Liquid–liquid transition and polyamorphism, J. Chem. Phys. 153 130901 (2020). https://doi.org/10.1063/5.0021045.

[53] E.G. Ponyatovsky, O.I. Barkalov, Pressure—induced amorphous phases, Mater. Sci. Reports. 8 (1992) 147–191. https://doi.org/10.1016/0920-2307(92)90007-N.

[54] P. Lucas, Fragile-to-strong transitions in glass forming liquids, J. Non-Crystalline Solids X. 4 (2019) 100034. https://doi.org/10.1016/j.nocx.2019.100034.

[55] C. Zhang, L. Hu, Y. Yue, J.C. Mauro, Fragile-to-strong transition in metallic glass-forming liquids, J. Chem. Phys. 133 (2010) 1–7. https://doi.org/10.1063/1.3457670.

[56] E. Rapoport, Model for Melting-Curve Maxima at High Pressure, J. Chem. Phys. 46 (1967) 2891–2895. https://doi.org/10.1063/1.1841150.

[57] E. Rapoport, Melting-Curve Maxima at High Pressure. II. Liquid Cesium. Resistivity, Hall Effect, and Composition of Molten Tellurium, J. Chem. Phys. 48 (1968) 1433–1437. https://doi.org/10.1063/1.1668858.

[58] E.G. Ponyatovskii, V. V Sinand, Second Critical Point an Low-temperature Anomalies in the Physical Properties of Water, JETP Lett. 60 (1994) 5.

[59] E.G. Ponyatovsky, T.A. Pozdnyakova, The T-P phase diagrams of amorphous GaSb, InSb and InAs, J. Non. Cryst. Solids. 188 (1995) 153–160. https://doi.org/10.1016/0022-3093(95)00092-5.

[60] E.G. Ponyatovsky, A thermodynamic approach to T – P phase diagrams of substances in liquid and amorphous states, J. Phys. Condens. Matter. 15 (2003) 6123–6141. https://doi.org/10.1088/0953-8984/15/36/304.

[61] C.T. Moynihan, Two Species/Nonideal Solution Model for Amorphous/Amorphous Phase Transitions, MRS Proc. 455 (1997) 411–425. https://doi.org/10.1557/PROC-455-411.

[62] C.A. Angell, C.T. Moynihan, M. Hemmati, `Strong' and `superstrong' liquids, and an approach to the perfect glass state via phase transition, J. Non. Cryst. Solids. 274 (2000) 319–331. https://doi.org/10.1016/S0022-3093(00)00222-2.

[63] H. Tanaka, General view of a liquid-liquid phase transition, Phys. Rev. E. 62 (2000) 6968–6976.

https://doi.org/10.1103/PhysRevE.62.6968.

[64] S. Strässler, C. Kittel, Degeneracy and the order of the phase transformation in the molecular-field approximation, Phys. Rev. 139 (1965) 3–5. https://doi.org/10.1103/PhysRev.139.A758.

[65] C.E. Bertrand, M.A. Anisimov, Peculiar Thermodynamics of the Second Critical Point in Supercooled Water, J. Phys. Chem. B. 115 (2011) 14099–14111. https://doi.org/10.1021/jp204011z.

[66] V. Holten, M.A. Anisimov, Entropy-driven liquid–liquid separation in supercooled water, Sci. Rep. 2 (2012) 713. https://doi.org/10.1038/srep00713.

[67] V. Holten, J.C. Palmer, P.H. Poole, P.G. Debenedetti, M.A. Anisimov, Two-state thermodynamics of the ST2 model for supercooled water, J. Chem. Phys. 140 104502 (2014). https://doi.org/10.1063/1.4867287.

[68] J.W. Biddle, R.S. Singh, E.M. Sparano, F. Ricci, M.A. González, C. Valeriani, J.L.F. Abascal, P.G. Debenedetti, M.A. Anisimov, F. Caupin, Two-structure thermodynamics for the TIP4P/2005 model of water covering supercooled and deeply stretched regions, J. Chem. Phys. 146 (2017). https://doi.org/10.1063/1.4973546.

[69] C.T. Moynihan, C.A. Angell, Bond lattice or excitation model analysis of the configurational entropy of molecular liquids, J. Non. Cryst. Solids. 274 (2000) 131–138. https://doi.org/10.1016/S0022-3093(00)00198-8.

[70] B. Wunderlich, STUDY OF THE CHANGE IN SPECIFIC HEAT OF MONOMERIC AND POLYMERIC GLASSES DURING THE GLASS TRANSITION, J. Phys. Chem. 64 (1960) 1052–1056. https://doi.org/10.1021/j100837a022.

[71] D. V. Matyushov, C.A. Angell, Gaussian excitations model for glass-former dynamics and thermodynamics, J. Chem. Phys. 126 094501 (2007). https://doi.org/10.1063/1.2538712.

[72] I.S. Klein, C.A. Angell, Excess thermodynamic properties of glassforming liquids: The rational scaling of heat capacities, and the thermodynamic fragility dilemma resolved, J. Non. Cryst. Solids. 451 (2016) 116–123. https://doi.org/10.1016/j.jnoncrysol.2016.06.006.

[73] C.H.P. Lupis, Chemical Thermodynamics of Materials, P T R Prentice-Hall, Inc., Englewood Cliffs, New-Jersey, 1983.

[74] S. Stølen, T. Grande, Chemical thermodynamics of materials: macroscopic and microscopic aspects, John Wiley & Sons Ltd., 2004.

[75] M.J. Cuthbertson, P.H. Poole, Mixturelike Behavior Near a Liquid-Liquid Phase Transition in Simulations of Supercooled Water, Phys. Rev. Lett. 106 115706 (2011). https://doi.org/10.1103/PhysRevLett.106.115706.

[76] P.B. Macedo, W. Capps, T.A. Litovitz, Two-State Model for the Free Volume of Vitreous B2O3, J. Chem. Phys. 44 (1966) 3357–3364. https://doi.org/10.1063/1.1727238.

[77] W. Kauzmann, Pressure effects on water and the validity of theories of water behavior, Colloq. Int. Du CNRS. 246 (1976) 63–71.

[78] S.M. Stishov, N.A. Tikhomirova, Phase diagram of tellurium, Sov. J. Exp. Theor. Phys. Lett. 22 (1966) 429–430.

[79] W. Klement, L.H. Cohen, G.C. Kennedy, Melting and freezing of selenium and tellurium at high pressures, J. Phys. Chem. Solids. 27 (1966) 171–177. https://doi.org/10.1016/0022-3697(66)90178-8.

[80] V. V. Brazhkin, R.N. Voloshin, S. V. Popova, A.G. Umnov, Pressure-temperature phase diagram of solid and liquid Te under pressures up to 10 GPa, J. Phys. Condens. Matter. 4 (1992) 1419–1425. https://doi.org/10.1088/0953-8984/4/6/006.

[81] V. Holten, J. Kalová, M.A. Anisimov, J. V. Sengers, Thermodynamics of liquid-liquid criticality in supercooled water in a mean-field approximation, Int. J. Thermophys. 33 (2012) 758–773. https://doi.org/10.1007/s10765-012-1195-z.

[82] F. Caupin, M.A. Anisimov, Thermodynamics of supercooled and stretched water: Unifying two-structure description and liquid-vapor spinodal, J. Chem. Phys. 151 034503 (2019). https://doi.org/10.1063/1.5100228.

[83] D.E. Hare, C.M. Sorensen, The density of supercooled water. II. Bulk samples cooled to the homogeneous nucleation limit, J. Chem. Phys. 87 (1987) 4840–4845. https://doi.org/10.1063/1.453710.

[84] W.M. Haynes, D.R. Lide, T.J. Bruno, CRC Handbook of Chemistry and Physics (2016-2017), 97th ed., CRC Press, n.d.

[85] M.A. Anisimov, A. V Voronel', N.S. Zaugol'nikova, G.I. Ovodov, Specific heat of water near the melting point and {O}rnstein-{Z}ernike fluctuation corrections, JETP Lett. 15 (1972) 317–319.

[86] C.A. Angell, W.J. Sichina, M. Oguni, Heat capacity of water at extremes of supercooling and superheating, J. Phys. Chem. 86 (1982) 998–1002. https://doi.org/10.1021/j100395a032.

[87] E. Tombari, C. Ferrari, G. Salvetti, Heat capacity anomaly in a large sample of supercooled water, Chem. Phys. Lett. 300 (1999) 749–751. https://doi.org/10.1016/S0009-2614(98)01392-X.

[88] D.G. Archer, R.W. Carter, Thermodynamic Properties of the NaCl + H2O System. 4. Heat Capacities of H2O and NaCl(aq) in Cold-Stable and Supercooled States, J. Phys. Chem. B. 104 (2000) 8563–8584. https://doi.org/10.1021/jp0003914.

[89] R.J. Speedy, C.A. Angell, Isothermal compressibility of supercooled water and evidence for a thermodynamic singularity at -45°C, J. Chem. Phys. 65 (1976) 851–858. https://doi.org/10.1063/1.433153.

[90] O. Mishima, Reversible first-order transition between two H2O amorphs at ~0.2 GPa and ~135 K, J. Chem. Phys. 100 (1994) 5910–5912. https://doi.org/10.1063/1.467103.

[91] G.P. Johari, Does water need a new Tg?, J. Chem. Phys. 116 (2002) 8067–8073. https://doi.org/10.1063/1.1466469.

[92] S. Capaccioli, K.L. Ngai, Resolving the controversy on the glass transition temperature of water?, J. Chem. Phys. 135 (2011) 104504. https://doi.org/10.1063/1.3633242.

[93] V. Velikov, S. Borick, C.A. Angell, The glass transition of water, based on hyperquenching experiments, Science (80-.). 294 (2001) 2335–2338. https://doi.org/10.1126/science.1061757.

[94] F.W. Starr, C.A. Angell, E. La Nave, S. Sastry, A. Scala, F. Sciortino, H.E. Stanley, Recent results on the connection between thermodynamics and dynamics in supercooled water, Biophys. Chem. 105 (2003) 573–583. https://doi.org/10.1016/S0301-4622(03)00067-X.

[95] P. Lucas, J. Pries, S. Wei, M. Wuttig, The glass transition of water, insight from phase change materials, J. Non-Crystalline Solids X. 14 (2022) 100084. https://doi.org/10.1016/j.nocx.2022.100084.

[96] F.P. Bundy, W.A. Bassett, M.S. Weathers, R.J. Hemley, H.U. Mao, A.F. Goncharov, The pressure-temperature phase and transformation diagram for carbon; updated through 1994, Carbon N. Y. 34 (1996) 141–153. https://doi.org/10.1016/0008-6223(96)00170-4.

[97] A.A. Correa, S.A. Bonev, G. Galli, Carbon under extreme conditions: Phase boundaries and electronic properties from first-principles theory, Proc. Natl. Acad. Sci. U. S. A. 103 (2006) 1204–1208. https://doi.org/10.1073/pnas.0510489103.

[98] M. Emuna, S. Matityahu, E. Yahel, G. Makov, Y. Greenberg, A reversible transition in liquid Bi under pressure, J. Chem. Phys. 148 (2018). https://doi.org/10.1063/1.5001916.

[99] L. Henry, M. Mezouar, G. Garbarino, D. Sifré, G. Weck, F. Datchi, Liquid–liquid transition and critical point in sulfur, Nature. 584 (2020) 382–386. https://doi.org/10.1038/s41586-020-2593-1.

[100] H. Tanaka, Bond orientational order in liquids: Towards a unified description of water-like anomalies, liquid-liquid transition, glass transition, and crystallization, Eur. Phys. J. E. 35 (2012) 113. https://doi.org/10.1140/epje/i2012-12113-y.

[101] M.A. Anisimov, M. Duška, F. Caupin, L.E. Amrhein, A. Rosenbaum, R.J. Sadus, Thermodynamics of Fluid Polyamorphism, Phys. Rev. X. 8 (2018) 1–18. https://doi.org/10.1103/PhysRevX.8.011004.

[102] P. Benigni, Thermodynamic analysis of the classical lattice-hole model of liquids, J. Non. Cryst. Solids. 534 (2020) 119942. https://doi.org/10.1016/j.jnoncrysol.2020.119942.